WL-TR-91-4036

SUPERVOLTAGE NDE TECHNIQUES FOR LARGE AEROSPACE STRUCTURES

Paul D. Tonner
James H. Stanley

Advanced Research and
Applications Corporation (ARACOR)
425 Lakeside Drive
Sunnyvale, CA 94086

July 1991

Final Report for Period February 1989 - January 1991

MATERIALS DIRECTORATE
WRIGHT LABORATORY
AIR FORCE SYSTEMS COMMAND
WRIGHT-PATTERSON AIR FORCE BASE, OHIO 45433-6533

NOTICE

When Government drawings, specifications, or other data are used for any purpose other than in connection with a definitely Government-related procurement, the United States Government incurs no responsibility or any obligation whatsoever. The fact that the government may have formulated or in any way supplied the said drawings, specifications, or other data, is not to be regarded by implication, or otherwise in any manner construed, as licensing the holder, or any other person or corporation; or as conveying any rights or permission to manufacture, use, or sell any patented invention that may in any way be related thereto.

This report is releasable to the National Technical Information Service (NTIS). At NTIS, it will be available to the general public, including foreign nations.

This technical report has been reviewed and is approved for publication.

Mark P. Blodgett 12 Aug 91

MARK P. BLODGETT
Nondestructive Evaluation Branch
Metals and Ceramics Division

Tobey M. Cordell

TOBEY M. CORDELL, Chief
Nondestructive Evaluation Branch
Metals and Ceramics Division

FOR THE COMMANDER

L R Bidwell

LAWRENCE R. BIDWELL, Deputy Director
Metals and Ceramics Division
Materials Directorate

If your address has changed, if you wish to be removed from our mailing list, or if the addressee is no longer employed by your organization please notify WL/MLLP, WPAFB, OH 45433-6533 to help us maintain a current mailing list.

Copies of this report should not be returned unless return is required by security considerations, contractual obligations, or notice on a specific document.

UNCLASSIFIED
SECURITY CLASSIFICATION OF THIS PAGE

REPORT DOCUMENTATION PAGE

Form Approved
OMB No. 0704-0188

1a. REPORT SECURITY CLASSIFICATION UNCLASSIFIED	1b. RESTRICTIVE MARKINGS
2a. SECURITY CLASSIFICATION AUTHORITY N/A SINCE UNCLASSIFIED	3. DISTRIBUTION/AVAILABILITY OF REPORT Approved for public release; distribution is unlimited.
2b. DECLASSIFICATION/DOWNGRADING SCHEDULE N/A SINCE UNCLASSIFIED	
4. PERFORMING ORGANIZATION REPORT NUMBER(S) FR743-91	5. MONITORING ORGANIZATION REPORT NUMBER(S) WL-TR-91-4036
6a. NAME OF PERFORMING ORGANIZATION ADVANCED RESEARCH AND APPLICATIONS CORPORATION 6b. OFFICE SYMBOL (If applicable)	7a. NAME OF MONITORING ORGANIZATION Materials Directorate (WL/MLLP) Wright Laboratory
6c. ADDRESS (City, State, and ZIP Code) 425 LAKESIDE DRIVE SUNNYVALE, CA 94086	7b. ADDRESS (City, State, and ZIP Code) WPAFB, OH 45433-6533
8a. NAME OF FUNDING/SPONSORING ORGANIZATION Materials Directorate 8b. OFFICE SYMBOL (If applicable) WL/MLLP	9. PROCUREMENT INSTRUMENT IDENTIFICATION NUMBER F33615-88-C-5511
8c. ADDRESS (City, State, and ZIP Code) AERONAUTICAL SYSTEMS DIVISION (AFSC) UNITED STATES AIR FORCE WRIGHT-PATTERSON AFB, OHIO 45433-6533	10. SOURCE OF FUNDING NUMBERS PROGRAM ELEMENT NO. 65502F; PROJECT NO. 3005; TASK NO. 52; WORK UNIT ACCESSION NO. 31
11. TITLE (Include Security Classification) SUPERVOLTAGE NDE TECHNIQUES FOR LARGE AEROSPACE STRUCTURES	
12. PERSONAL AUTHOR(S) Paul D. Tonner, James H. Stanley	
13a. TYPE OF REPORT Final	13b. TIME COVERED FROM 890208 TO 910128
14. DATE OF REPORT (Year, Month, Day) 91/07/17	15. PAGE COUNT 47
16. SUPPLEMENTARY NOTATION	

17. COSATI CODES		
FIELD	GROUP	SUB-GROUP

18. SUBJECT TERMS (Continue on reverse if necessary and identify by block number)
supervoltage computed tomography, nondestructive evaluation, solid rocket motors

19. ABSTRACT (Continue on reverse if necessary and identify by block number)

Innovative technical approaches for detecting and characterizing defects in aerospace structures like large solid rocket boosters or jet engines are urgently needed. Unfortunately, in fully assembled components, zones which are the most critical to system reliability are often the most inaccessible to standard examination techniques. A computed tomography (CT) system can provide excellent images of otherwise inaccessible areas but the size and opacity of large aerospace components preclude the use of even the most energetic industrial CT systems produced to date. If the power of CT is to be extended to the largest solid rocket boosters and other large aerospace structures, bremsstrahlung radiation with peak energies in the 40- to 60-MV range is required. The use of these "supervoltage" energies for CT completes the logical extension of CT to the highest practical energies since material attenuations begin to increase for higher energies. A Phase I effort verified the feasibility of the concept by resolving key questions relating to operation at supervoltage energies. The key objective of the Phase II program was to obtain a supervoltage CT image of an aerospace structure which, because of its size and opacity, could not be imaged with current CT technology. Supervoltage CT images of many configurations of a simulated 3.9-m-diameter, 12-mm steel case solid rocket booster, obtained on a pre-prototype supervoltage CT scanner specially

20. DISTRIBUTION/AVAILABILITY OF ABSTRACT ☒ UNCLASSIFIED/UNLIMITED ☐ SAME AS RPT ☐ DTIC USERS	21. ABSTRACT SECURITY CLASSIFICATION UNCLASSIFIED
22a. NAME OF RESPONSIBLE INDIVIDUAL MARK P. BLODGETT	22b. TELEPHONE (Include Area Code) 513-255-9805 22c. OFFICE SYMBOL WL/MLLP

DD Form 1473, JUN 86 *Previous editions are obsolete.*

SECURITY CLASSIFICATION OF THIS PAGE
UNCLASSIFIED

Block 19. ABSTRACT (continued)

designed for this purpose, conclusively demonstrate that supervoltage CT is feasible and completes the extension of CT to the highest possible X-ray energies. Furthermore, analysis of the supervoltage images provides convincing evidence that CT dynamic range, contrast sensitivity and defect detectability are not diminished, and may in some cases be enhanced, at supervoltage energies.

TABLE OF CONTENTS

Figures **Captions** **Page**

LIST OF FIGURES

LIST OF FIGURES

LIST OF TABLES

ACKNOWLEDGEMENTS

Many talented managers, scientists, engineers and technologists contributed to the initiation and success of this work. The authors are pleased to acknowledge the efforts of Don Forney and his colleagues at WRDC who supported the supervoltage concept, arranged for project funding, and provided much appreciated assistance and encouragement during the course of the program. The work reported here was preceded by a Phase I project, also sponsored by WRDC, and executed by ARACOR physicists Ed Franco, Russel Stachowski and Jim LePage, all of whom made significant contributions to the present study. ARACOR engineers Kevork Derbedrossian and Victor Hu provided the considerable mechanical, electrical and electronic design expertise needed for a project of this nature. The ARACOR software team of Sanaa Fawzy, Victor Hu, Andrew Holland and Bill James succeeded in defining the requirements and developing software that met or exceeded all expectations. Experimentalists Hu, James, Holland and Bart Jackson worked long hours and with much creativity at the RPI Linac to assemble and commission the scanner and to obtain the results reported herein; all in a period of less than 20 working days. Andrew Holland completed the data analysis at ARACOR, making key contributions to the understanding of background effects, dynamic range compensation, beam hardening and region of interest reconstruction.

The supervoltage project could not have been a success without the extraordinary help of the staff at the RPI Linac. This included many discussions concerning source characteristics and shielding requirements with Linac directors Dr. Robert Block and Dr. Jim Howard. Linac Supervisor Jim Westhead made numerous arrangements and helpful technical suggestions and Technical Specialist Peter Brand made key contributions to the source pulsing design. Westhead, Brand and Technicians Matt Gray and Larry Prince provided experimental assistance at every opportunity, on several occasions working around the clock to keep the project on schedule. Image analysis performed by research student Aaron Dentinger provided the first quantitative evidence of the extraordinary sensitivity and linearity of the attenuation measurements, giving a much needed boost to the experimentalists. During the course of the experiment, many parts had to be fabricated on short notice. The design talent and many helpful suggestions of Linac machinist Jim Kelly were very much appreciated. Linac scheduling arrangements and coordination provided by Elaine Belokopitsky, Assistant to the Director, made it possible to rapidly and smoothly adjust to the many small changes in plan that occurred during the experiment.

1.0 INTRODUCTION

Currently available nondestructive examination (NDE) techniques are not able to efficiently assess the structural integrity and geometric characteristics of many large, fully assembled and highly attenuating aerospace structures. Aerospace structures in these categories include steel-case solid rocket motor (SRM) boosters such as the Titan 4 (3 m diameter) and space shuttle (3.6 m in diameter), nozzle components associated with SRM's of that size, assembled high-pressure cryogen pumps, and any of the large jet engines used on military and commercial aircraft. The composition, construction and size of these objects, coupled with the inaccessibility of some of the critical inspection zones (such as bonded surfaces in the Y-joint and restricter regions of SRM's), often preclude the use of current NDE techniques such as ultrasonics and conventional radiography. Thus, for these large and highly attenuating objects, innovative technical approaches are urgently needed to provide NDE data to support reliable structural integrity assessments.

The field of NDE has expanded rapidly in recent years with the introduction of a number of new techniques. One of the most important of the new NDE technologies is computed tomography (CT). CT, which began as a medical diagnostic tool, is rapidly becoming accepted in the industrial world whenever the objective is to nondestructively detect, locate and measure the size of material anomalies. A prominent early application of industrial CT is the inspection of SRM's and rocket nozzle components. The largest CT scanners currently installed are capable of inspecting the Trident (2.1-m diameter) and the Peacekeeper (2.4-m diameter) SRM's, both of which have composite cases. Scanners designed for these tasks use a 16-MV linear accelerator source. Other scanners using 9, 2 and 0.42 MV sources have also been designed for smaller objects.

If the power of CT is to be extended to the largest steel-case SRM's and other large aerospace structures, energies even higher than 16 MV must be used. The CT demonstration described in this report establishes the enabling technology which makes the extension of CT to highly attenuating objects possible. To accomplish this, bremsstrahlung radiation with peak energies in the 40 to 60 MV range is used. Because the concept involves the use of X-rays with energies significantly higher than have previously been employed, this approach has been designated "supervoltage CT" or "SVCT," and the energy regime of interest is referred to as the "supervoltage" regime. Supervoltage CT extends source energies to the point where no further increase in X-ray energy provides improvement in performance because, at energies above the supervoltage regime, material attenuations cease decreasing and begin to increase without bound with increasing energy (Figure 1).

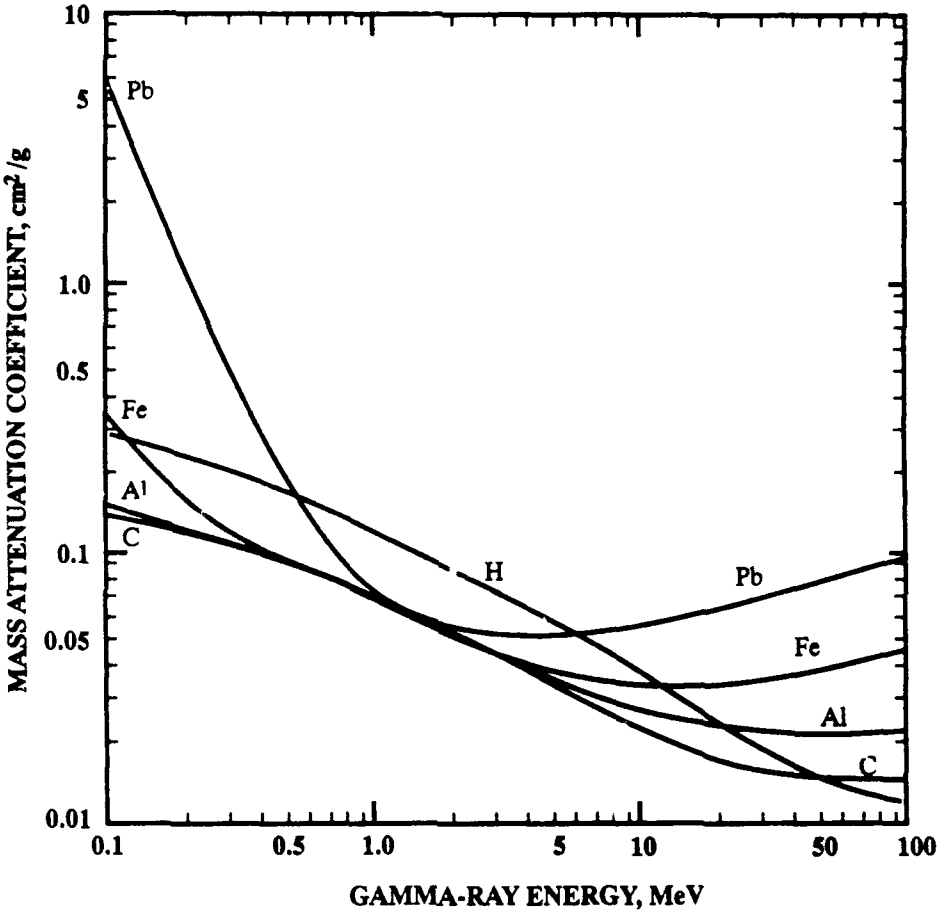

Figure 1. Mass attenuation coefficient as a function of energy for some common elements.

Initial computer calculations of the transport of supervoltage bremsstrahlung radiation through thicknesses of steel and propellant appropriate to large aerospace components provided very encouraging results. However, these calculations represented a necessary but not sufficient condition for establishing the feasibility of the supervoltage CT concept. Other less easily calculated, but equally important, effects become significant in the supervoltage X-ray regime. These include pair production, scatter, buildup, and photo-induced radioactivity. The magnitude and characteristics of these radiation phenomena are highly dependent on materials and geometry and can introduce nonlinear effects into the measurement. Another concern in scanning large objects is that the dynamic range of the detector and data acquisition electronics limit the attenuation range which the system can accommodate. The nonlinear effects associated with the supervoltage energy regime impose engineering difficulties on the interpretation of the transmitted signal and these, in turn, impose limitations on the ultimate attenuation range achievable by such an imaging system.

Supervoltage bremsstrahlung sources are available in large laboratory facilities but are restricted by size and power limitations. The extension of practical CT to the supervoltage regime will require the evolution of new compact supervoltage X-ray sources. The recent emergence of the 50-MV racetrack linear accelerator source as a commercially available product is an important development that will greatly enhance the practicality and effectiveness of supervoltage CT.

A Phase-I proof-of-feasibility study was performed to determine if any of the radiation phenomena in question could prevent supervoltage CT from achieving its promise. Experiments were designed to determine if the high quality attenuation measurements upon which CT depends would be compromised at supervoltage energies by photo-activation, scintillator performance, anomalous buildup or other background noise problems. These tests were carried out using the 60-MV LINAC at Rensselaer Polytechnic Institute's Gaerttner Laboratory in Troy, New York. The magnitude and characteristics of the nonlinear effects were the subject of the Phase I project. The results of the measurements made during the course of that study were the first definitive affirmation of the feasibility of a supervoltage CT inspection system. The Phase I work was performed under Contract # F33615-87-C-5273 for the Materials Laboratory, AFWAL, Wright-Patterson AFB. More detail is given in the final report for that project (ARACOR Report # FR-88-604). The data and major conclusions of the Phase I project were reviewed before proceeding with Phase II work and the findings of that review are summarized in Table 1.

Table 1. Phase I Review Findings.

1. The Phase I attenuation measurements were influenced by scatter, buildup and background in a way that suggested additional collimator and shielding design effort was required in order to achieve useful CT measurements.
2. Induced radioactivity in propellant does not present a materials or a health physics problem.
3. Induced activity in the scintillator crystals does not interfere with the attenuation measurements or cause any measurable darkening of the crystals.

The thrust of the Phase II effort was to implement at RPI a pre-prototype CT system, including detector package and handling mechanism and scan an appropriately challenging test article. A CT image obtained with this equipment demonstrates the proof of principle of supervoltage CT and establishes it as a viable NDE inspection technique for highly attenuating objects. To be convincing, the demonstration required the use of an object equivalent to a full-sized aerospace component such as a solid rocket booster or jet engine. In this way, the

engineering difficulties presented by a supervoltage CT system are addressed and finer phenomenological details are identified as a consequence of implementing an entire data chain from measurement to image. The experience of determining supervoltage imaging requirements additionally serves as guidance for the design of a full-up supervoltage CT system. The goals and objectives of the Phase-II program are summarized in Table 2.

Table 2. Goals and Objectives of the Phase-II Program.

1.	Build a demonstration supervoltage scanner
2.	Install the scanner at the RPI Linac, Troy, New York
3.	Obtain a supervoltage image of an aerospace structure which, because of its size, could not otherwise have been imaged with existing CT equipment
4.	Evaluate the image accuracy
5.	Determine any fundamental limitations of supervoltage CT
6.	Investigate issues associated with full-up design

The SVCT project posed a number of practical difficulties, stemming primarily from the fact that system integration could not be completed until all equipment arrived at RPI and secondarily from the tight experimental schedule at RPI. The experimental test plan that was included in the March 25, 1990 Technical Operating Report is outlined in order of priority in the Appendix. The actual work proceeded more or less along these lines, tackling the highest priority tasks first. Although some of the lower priority items, which ideally the program would have liked to address, could not be completed within the funds available, the Phase II effort successfully accomplished all of the key technical objectives that had been set. The specific benefits which motivated this work are an expanded range of CT applications and the extension of CT technology to the maximum possible X-ray source energies. These primary benefits of SVCT are summarized in Table 3:

Table 3. Primary Benefits of SVCT.

1)	The extension of X-ray imaging to the highest possible energies;
2)	The optimal maintenance of higher-Z, assembled objects consisting of up to the equivalent of 60 centimeters of steel; and
3)	The ability to image objects consisting of lower-Z material equivalent to 4 meters of solid propellant.

In the course of the Phase II effort, five additional benefits of SVCT were conceived. The first is that, while supervoltage CT is not necessary for smaller, less attenuating objects, it can often be applied to these objects with better results than would be achieved at lower energies. This is because the high photon flux of a supervoltage CT source (high because the efficiency of the source target increases with electron energy) will often result in a net improvement in signal-to-noise ratio compared to that which can be achieved with 2- to 15-MV sources.

The second unanticipated benefit is that high a resolution could be engineered using a supervoltage source. This is because the high photon flux of the supervoltage source and the high penetration of the supervoltage photons would, to an extent, compensate for the reduction in signal that would occur if a large source-to-detector distance caused by the and narrow apertures.

The third additional benefit not originally anticipated is that, for effective energies above about 10 MV and for materials with Z less than about 13 (i.e., less than the Z of Al), artifacts due to beam hardening are minimized. The reason for this is that the mass attenuation coefficients for these materials in that energy range are virtually independent of energy (see Figure 1).

The fourth unanticipated benefit is that for effective energies above about 5 MV, the relative contrast (i.e., the relative mass attenuation coefficients) for materials with Z less than about 26 (i.e., less than that of Fe) begins to improve with increasing energy. For many materials, the contrast between materials at 20 MV can only be matched at energies below 70 kV, an energy which is too low to inspect many items of practical interest.

The fifth unanticipated benefit is that it should be possible to obtain two separate, low-noise images; one primarily sensitive to elemental composition and the other primarily sensitive to density distribution, using a supervoltage dual-energy technique. This technique would be similar to the dual-energy technique performed at lower energies, except for the fact that it would not be hampered by a lack of adequate photon statistics nor restricted to smaller, low-Z objects. The reason for this is that the two energies that would be used are both relatively high, allowing ample penetration through even large high-Z objects. The lower effective energy would be in the 1- to 5-MV range (where attenuation is dominated by the density-dependent Compton effect) and the upper effective energy would be in the 5- to 50-MV range (where attenuation is dominated by the Z-dependent pair production effect). Possible applications for a SVCT dual-energy technique include, but are not limited to, the detection of chlorine migration and aging effects in SRM propellant, the detection and in-process monitoring of elemental composition distributions in advanced ceramics and composites, the detection of residual core in cast turbine blades, the

migration of fluids and high-Z components in soil test beds, the inspection of nuclear fuel waste drums, the detection of explosives, munitions and contraband in rail cars luggage and the detection of aging effects in aircraft.

The additional benefits of supervoltage CT not originally anticipated are summarized in Table 4.

Table 4. Secondary Supervoltage CT Benefits.

1. Supervoltage CT of small objects can result in better contrast sensitivity than can be achieved at lower energies
2. High resolution scanning should be possible using supervoltage sources
3. Artifacts due to beam hardening are minimized for effective energies above about 10-MV and for materials with Z less than about 13
4. Relative contrast is improved between materials for effective energies above about 5 MV and for materials with Z less than about 26
5. Separation of elemental and density composition should be possible using a supervoltage dual-energy technique

The selected supervoltage phantom is described in Section 2 and the experimental apparatus used to scan it is reviewed in Section 3. Scan results are presented in Section 4 together with analysis of the accuracy of the images. Conclusions and recommendations for additional supervoltage development are summarized in Section 5.

2.0 PHANTOM

The successful development of supervoltage CT will open up inspection applications previously considered impossible due to the limitations of standard CT techniques. The realm of critical structures (i.e., structures requiring high-confidence NDE) that can not be inspected with existing CT technology can be divided into two basic categories: (1) large objects such as SRM's which contain low-Z materials and are highly attenuating by virtue of sheer size, and (2) smaller objects such as jet engines which contain higher-Z materials and are highly attenuating by virtue of their mass and atomic number. The requirements for the inspection of these important types of aerospace structures are the driving force behind the development of the supervoltage CT technique.

Transatmospheric vehicles which will be able to transport large loads into space and back are unlikely to become a practical reality until well into the next century. For at least the remainder of this century, the only viable means for putting large payloads into orbit will be conventional rocket technology. The current strategy for orbiting large payloads involves the use of a large main liquid thruster in combination with two or more SRM boosters. The reliability of both types of motors is of paramount importance; innovative technical approaches for detecting and characterizing bulk defects are urgently needed. The design approach favored by the United States for some rockets systems, like Titan, is a configuration which employs only two large SRM boosters. The use of just two boosters, as opposed to a greater number of smaller ones, requires that their size must be substantial. The sheer size of these boosters, their construction and their chemical composition pose a challenging problem to NDE systems designers. It is believed, however, that CT can detect many of the known critical defects. The use of supervoltage energies to examine large rocket boosters using CT is one of the most exciting possibilities addressed by the supervoltage technique.

The second category of aerospace structures requiring an inspection technique such as supervoltage CT are compact, high density components such as assembled jet engines. These components require a high degree of reliability, and as engine power increases, so does the reliability requirement. The NDE problem is compounded by a corresponding increase in size and density of interior components. Supervoltage offers the promise of developing an optimal maintenance technique allowing one to observe interior components while they are still imbedded in their envelope of superalloy and steel. Assembled high pressure pumps, such as the Centaur, and power heads for cryogen distribution pose similar difficulties for present NDE inspection techniques. Assembly, disassembly and subsequent reassembly of these pumps is a painstaking and costly task when required to maintain the critical integrity of interior components. If a CT

technique can be brought to bear on the problem, in-service inspection of these structures could be made substantially more efficient and the final assembly much more reliable.

To meet the objectives of the supervoltage project and to demonstrate supervoltage CT in the most convincing manner, it was decided that the test object, or phantom, be larger than anything that could be scanned with existing CT scanners. The test object chosen for this purpose was a simulation of a 3.9-m SRM with a 12.7-mm steel case (Figure 2). An SRM of this size is significantly larger than the Titan SRM (3-m diameter) and slightly larger than the space shuttle SRM (3.6-m diameter).

While the phantom was radiographically equivalent to a 3.9 m SRM, its diameter and length were reduced to 1.8 m and 25 cm, respectively (Figures 3), so that it could fit through the radiation bay access door at the RPI facility. Size reduction also helped to keep handling problems manageable and to keep scanning equipment costs to a reasonable level.

To achieve the reduction in diameter while preserving radiographic equivalence, the linear attenuation coefficient of the simulated propellant was increased proportionately. To accomplish this, a systematic search for an exceptable radiographic equivalent was conducted. The material ultimately chosen to simulate the propellant was a mixture of cement and iron (60% cement, 40% iron). The mass attenuation coefficient of this mixture is about 1.3 times larger than that of

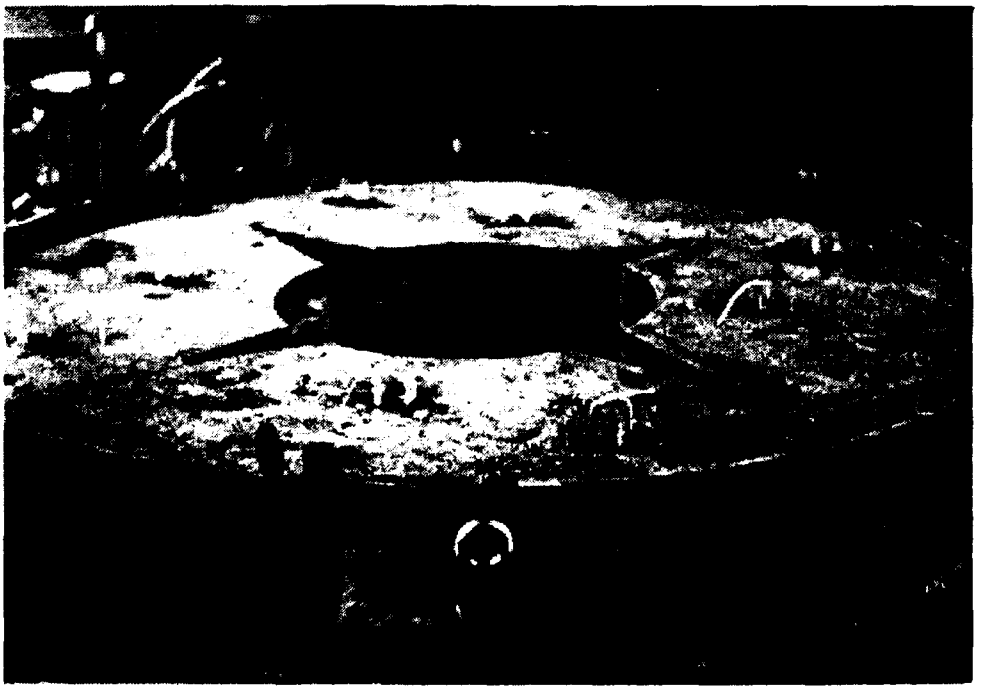

Figure 2. Photograph of the supervoltage CT test phantom.

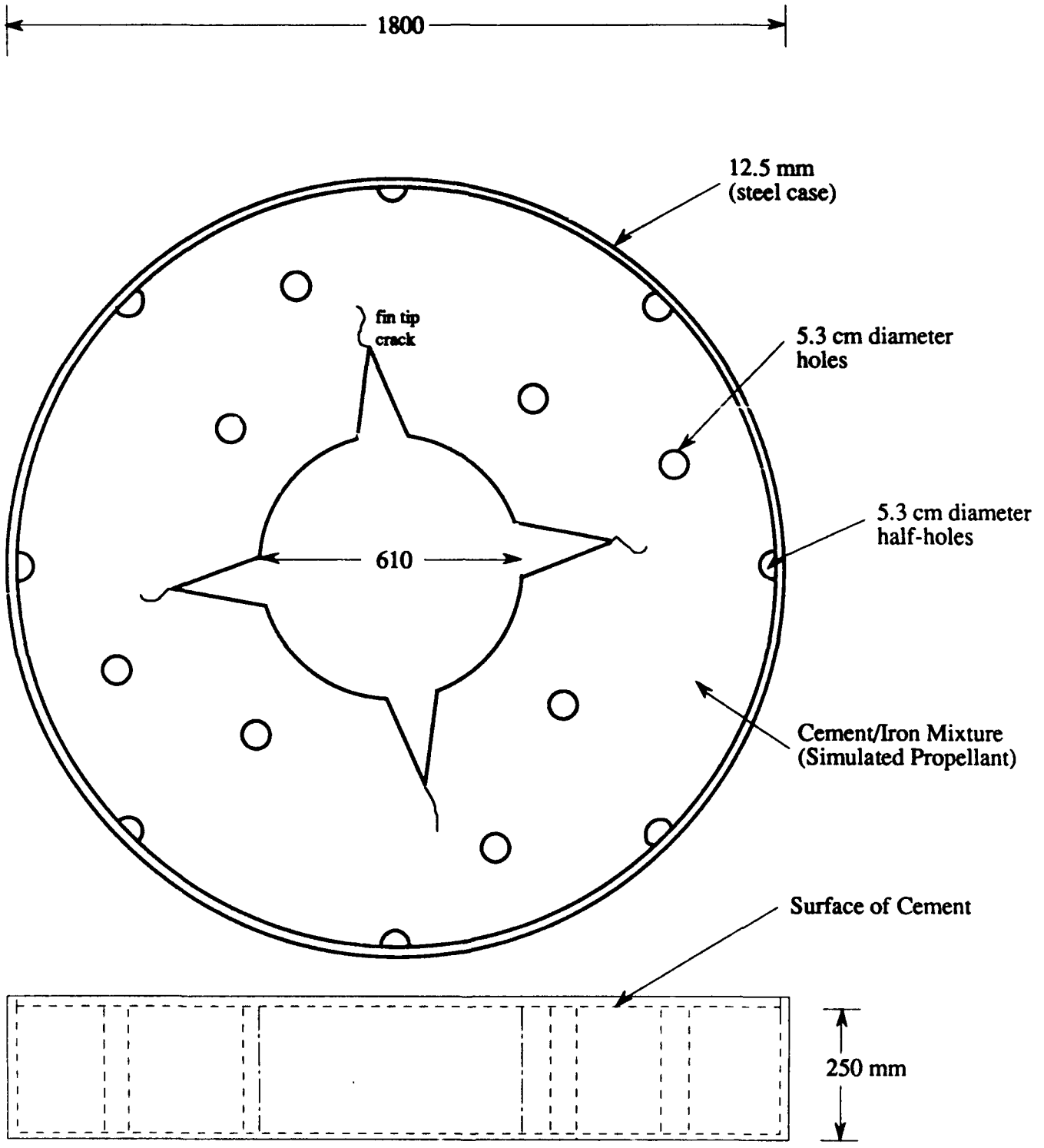

Figure 3. Schematic illustration of the test phantom.

propellant but varies with energy in about the same way as propellant (Figure 4). The cement-iron mixture has a density of about 3 g/cc; 1.7 times larger than the density of real propellant (1.8 g/cc). The linear attenuation coefficient of the phantom, which is given by the product of density and mass attenuation coefficient, is therefore about 2.2 times that of propellant (1.7 x 1.3). Consequently, the phantom diameter can be reduced to about 1.8-m (3.9/2.2) while maintaining the same radiographic thickness as a 3.9-m SRM.

The 25-cm thickness of the phantom was large enough, relative to the 2.5-cm CT slice thickness, to simulate the out-of-plane X-ray scatter behavior of a full-length SRM but not so thick as to be too heavy for the scanning mechanism. Even with the reduced diameter and thickness, the total weight of the phantom was in excess of 2000 kg.

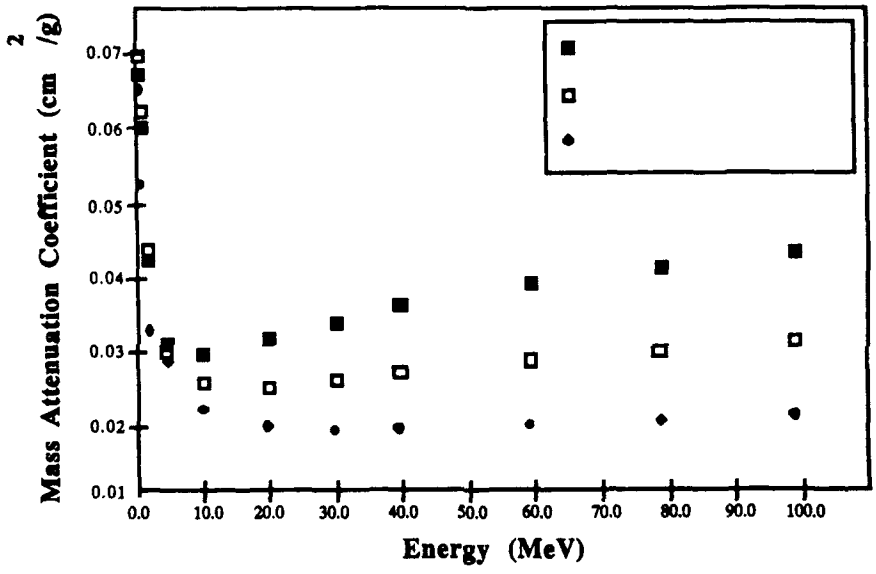

Figure 4. Mass attenuation coefficient as a function of energy for propellant, iron and the cement/iron mixture used in phantom.

To further simulate an actual SRM, the phantom was designed with a typical SRM center bore and fin pattern. Cracks starting at the fin tips, a common problem in SRM manufacture, were induced when the concrete-iron mixture was poured. A number of 5.3-cm-diameter holes were left in the phantom. These holes were designed to accept inserts. A variety of insert materials were selected, including wood, water, graphite, lucite, PVC, teflon, titanium, inert propellant and other miscellaneous low-Z and high-Z materials. Semicircular holes against the inner surface of the steel case were designed to accept simulated debonds at the case-to-insulator and insulator-to-propellant interfaces. The debonds were made in semi-circular inserts constructed of aluminum (to simulate the propellant) and Delrin plastic (to simulate the insulator) (Figure 5).

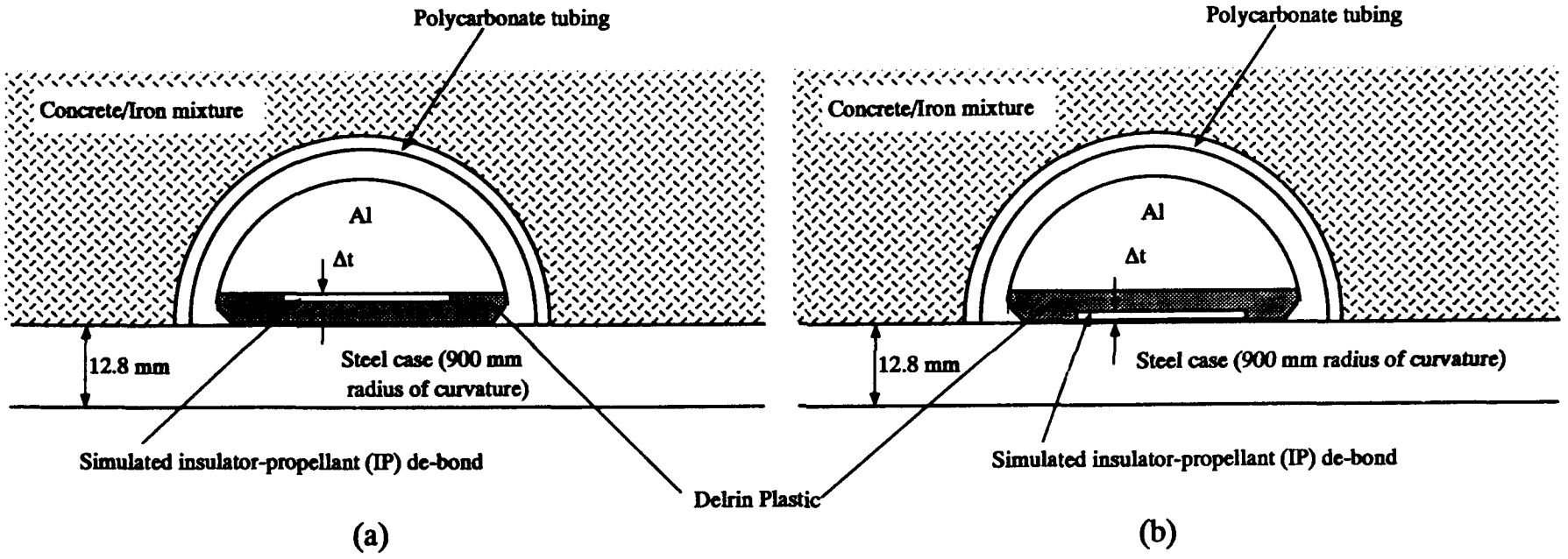

Figure 5. Schematic of inserts at periphery of phantom used to simulate (a) insulator-propellant (IP) and (b) insulator-case (IC) debonds.

3.0 APPARATUS

3.1 Source

The source of the supervoltage X-rays was the 60-MV linear accelerator (linac) at the Gaerttner Laboratory of the Rensselaer Polytechnic Institute (RPI) in Troy, New York (Figure 6). The linac is an L-band microwave electron accelerator with seven accelerating sections and a maximum energy of 60 MV. Typical operating conditions used for the CT scans were 60-MV peak energy, 1-μs pulse width, 100-Hz pulse frequency and an average current of 15 μA.

The source target was a series of four tantalum plates enclosed in an aluminum jacket and cooled with tap water (Figure 7). The flat face of the target was positioned 37 mm away from the end of the electron beam vacuum line (Figure 8). The 60-MV electrons passed through a thin window at the end of the beam line, traveled through the air and collided with the tantalum target to create bremsstrahlung X rays with a peak energy of 60 MV. Based on a CT slice thickness measurement, the source focal spot was estimated to be about 20 mm in diameter.

The target was mounted on a linear stage oriented along a line parallel to the axis of the electron beam. Detector signal was maximum when the target was located such that the focal point projected back from the detector apertures fell anywhere in the half of the target closest to the detector. The signal dropped 5 to 10% when the target was moved 6 mm outside of this envelope in either direction.

A thermocouple probe placed in a hole in the lead collimator about 10 cm from the front face of the target indicated a temperature of about 100°C under typical scan conditions. In the course of the experiments, thousands of kilograms of lead bricks and iron aggregate concrete blocks were stacked around the target area (Figure 9) to reduce background X-ray radiation in the reference and signal detectors. After reduction of X-ray background to its lowest possible level, the desired low background levels in the detectors were finally achieved with the addition of numerous blocks of borated polystyrene around the source target and detector areas. These "borated-poly" blocks absorbed neutrons which were being produced by γ-n reactions in the target and shielding.

3.2 Scanner

The scanner constructed for the supervoltage demonstration experiment was a second generation translate-rotate design employing eight signal detectors and one reference detector (Figure 10). The system comprised of source and detector collimators, a large translate-rotate

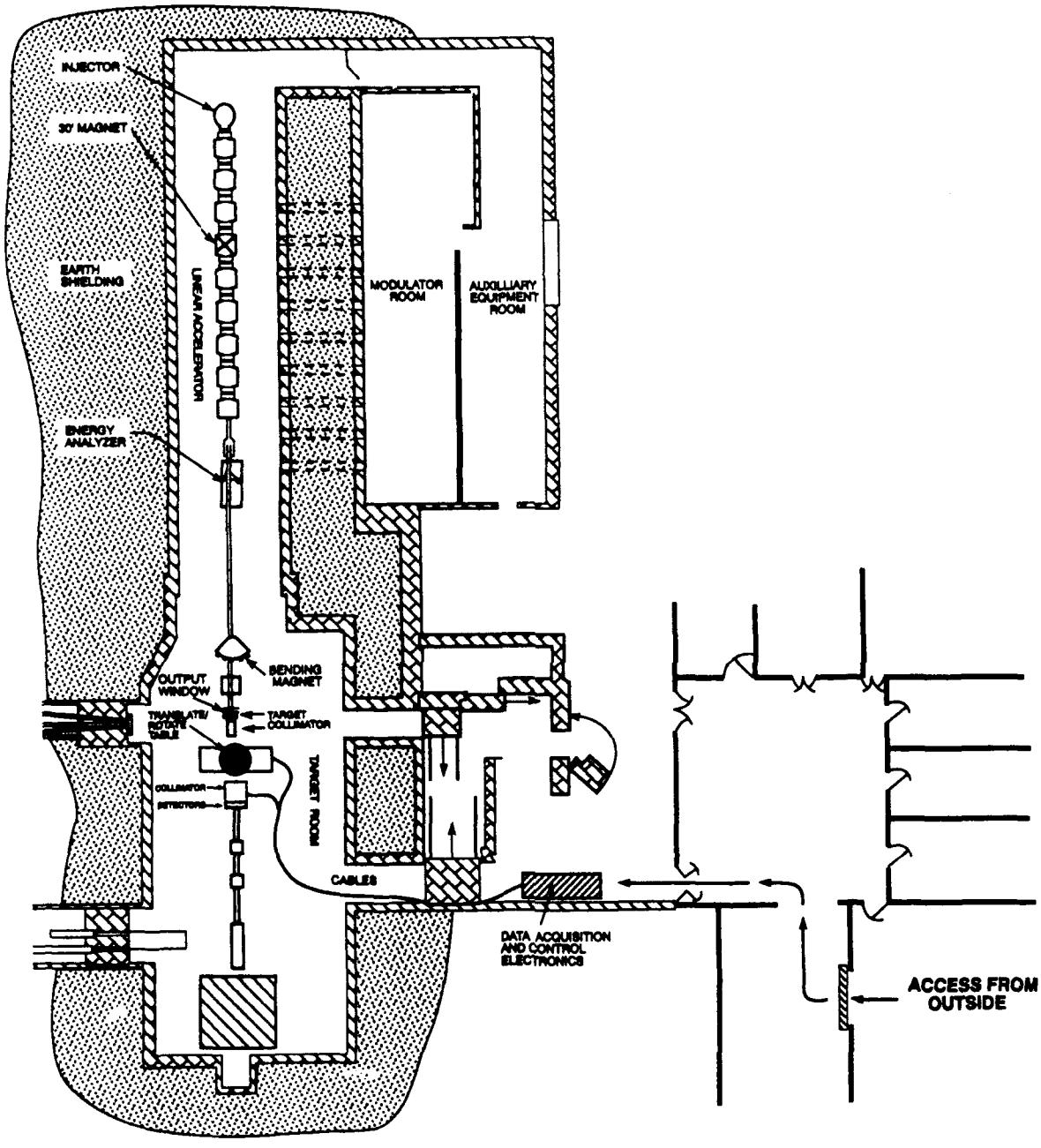

Figure 6. RPI Linac facility layout.

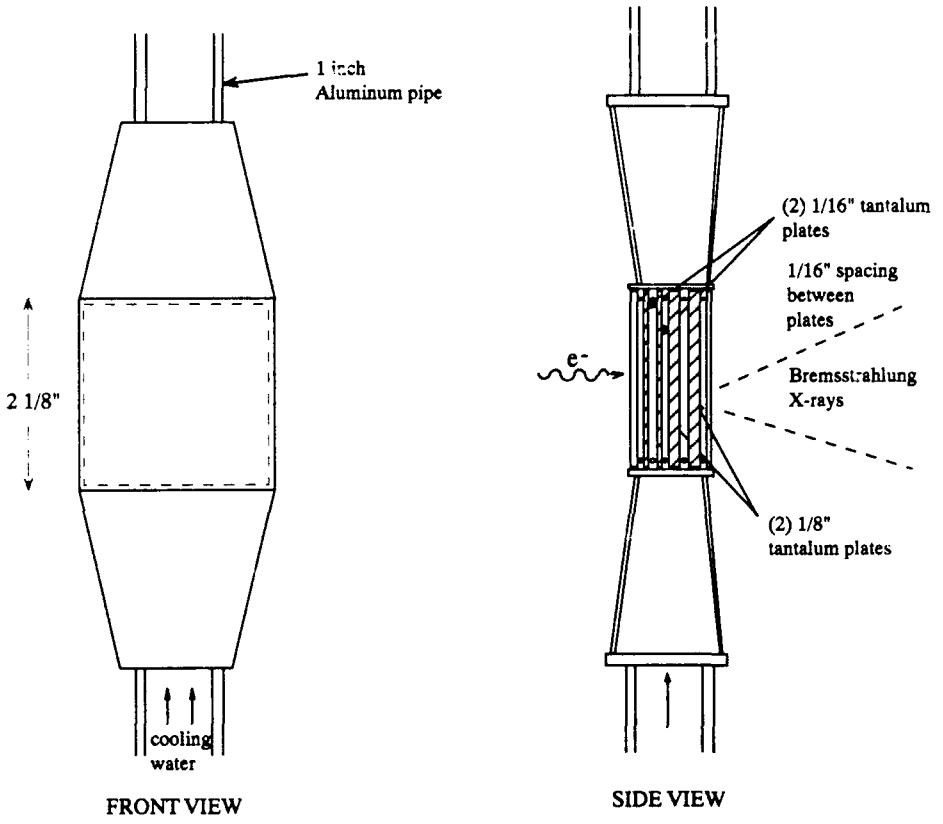

Figure 7. Schematic of tantalum target used for generating X-rays from electrons.

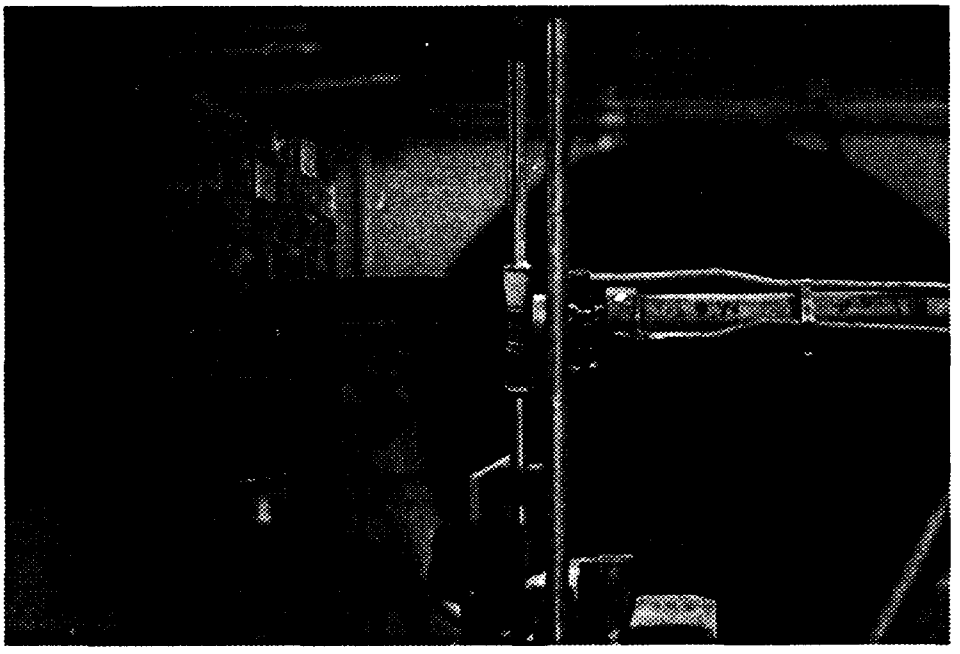

Figure 8. Photograph of the tantalum target before addition of shielding.

Figure 9. Photograph of target enclosed in stacked lead and iron-agregate block shielding

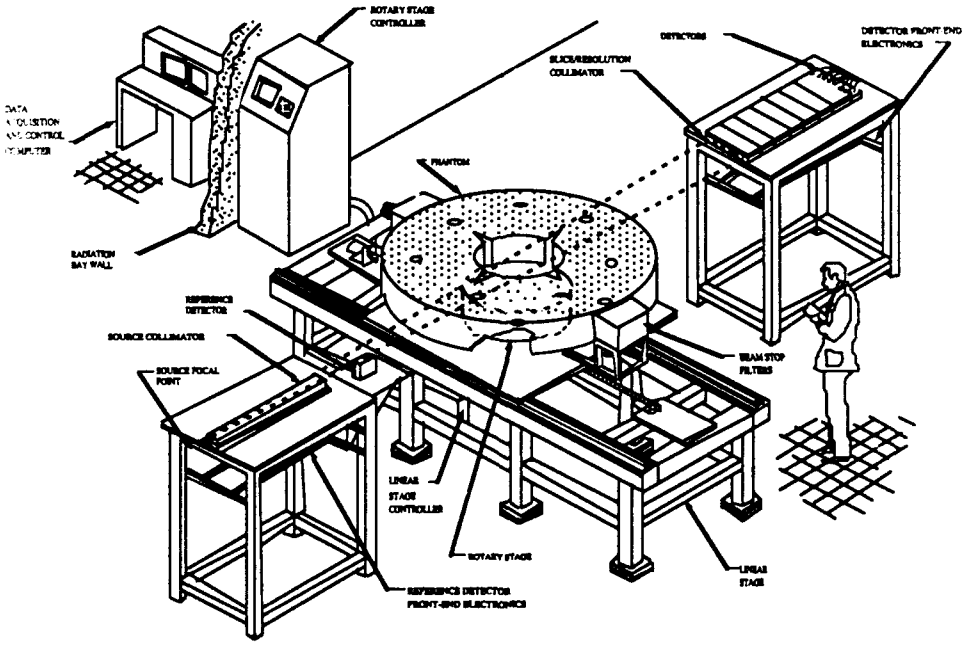

Figure 10. Schematic of supervoltage CT demonstration scanner.

mechanism (rotation table is partially hidden by the phantom in Figure 10), the reference detector and the eight signal detectors. The front-end electronics of the detectors were mounted under the detectors and connected to the data acquisition and control station outside the bay by 50-m-long fiberoptic cables. The scanner motion and source pulsing were synchronized with detector readings by the data acquisition and control system.

The translation table (see Figure 11, which shows the translate table being placed in the radiation bay) moved the object through the eight collimated X-ray beams 90 times in the course of a single scan. Between traverses, the object was rotated through a total of 180°. The combined motions produced a total of 720 parallel projections, each separated by 0.25°. To limit the dynamic range of the signals, all measurements were made relative to the signal transmitted through the two beam stop filters shown in Figure 10, rather than through air. The known attenuation due to the filters, which are 30-cm-thick pieces of iron, was subtracted from the scan data before reconstructing. By using these filters the dynamic range of the signal was reduced from six to three or four orders of magnitude. Since all measurements were made through a minimum of 30 cm of steel, the beam stop filters also acted to reduce beam hardening artifacts.

X-ray collimators were used on both the source and detector side of the object to form eight individual X-ray beams. Each collimator was 1 m long and constructed of machined lead blocks laid out on heavy-duty steel tables. The apertures in the collimators were machined such that all apertures pointed to the focal spot of the source when the equipment was properly aligned. The source-to-detector distance was 6 m, and the center of rotation was at the midpoint (Figure 12). The 6-m separation was about equal to the separation required to scan a full-size 4-m-diameter SRM. Hundreds of lead bricks, not shown in Figure 12, were placed around the reference detector and electronics (Figure 13) and around the signal detectors and electronics (Figure 14) to reduce background in the detectors and the possibility of radiation damage to the electronics. Borated polystyrene, not shown in Figures 13 and 14, was also eventually added to reduce background caused by neutrons.

The detectors used were an ARACOR-designed $CdWO_4$ scintillator connected to a photodiode through a fiber-optic prism. The signals were digitized in the radiation bay and carried over fiber-optic links to the computer station outside the bay. Data acquisition and control (DAAC), image reconstruction, image display and image analysis were accomplished by means of a pair of 386-based computers equipped with specialized circuitry, array processors and a Matrox image display board. The DAAC portion of the system is schematically illustrated in Figure 15.

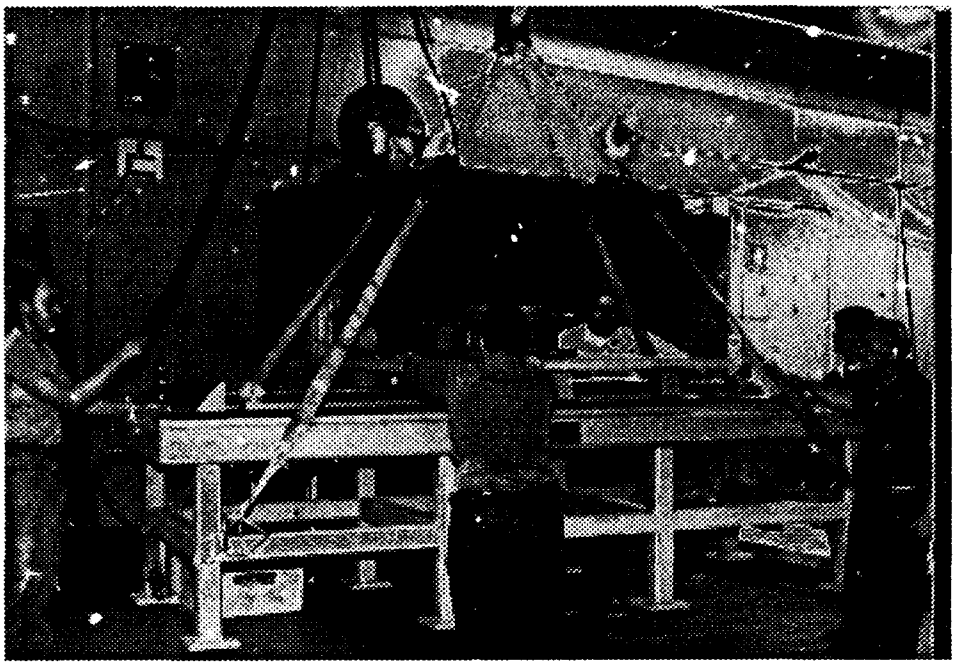

Figure 11. Positioning of the translate-rotate table in the radiation bay.

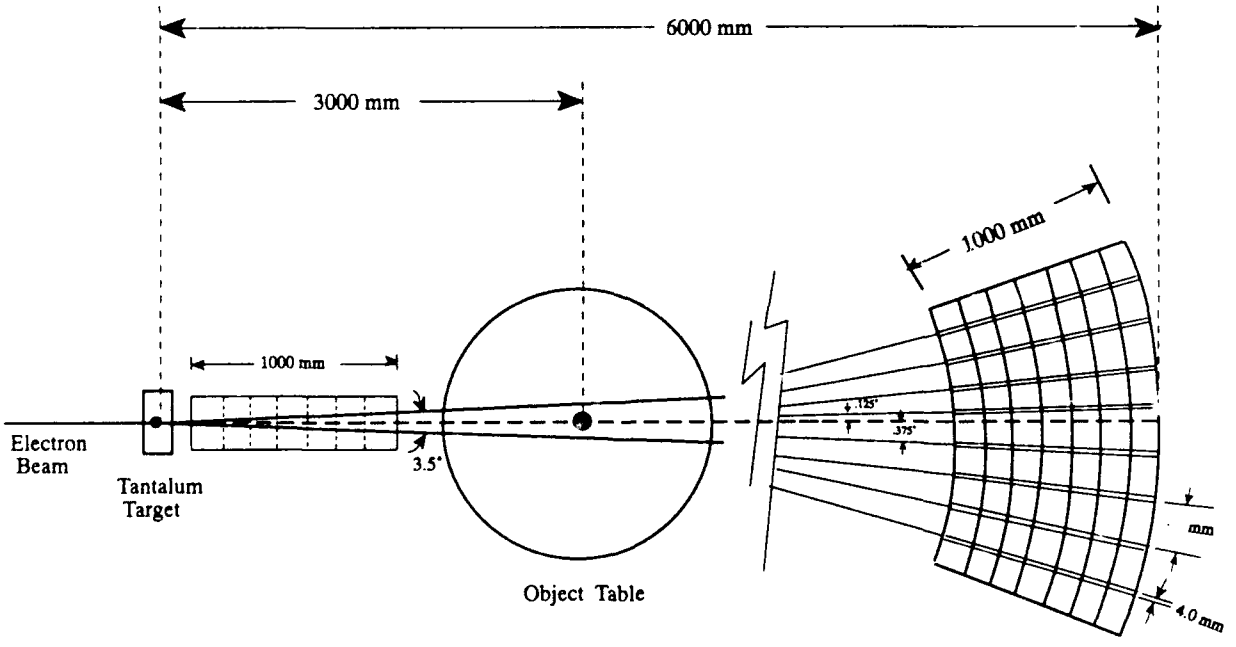

Figure 12. Dimensions and collimation for supervoltage demonstration scanner.

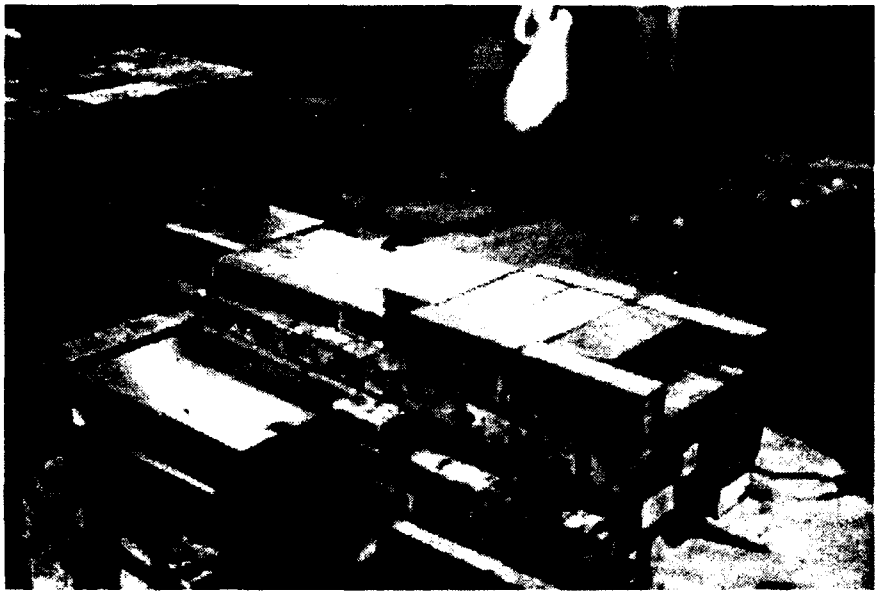

Figure 13. Photograph of the shielding around the source collimator and reference detector.

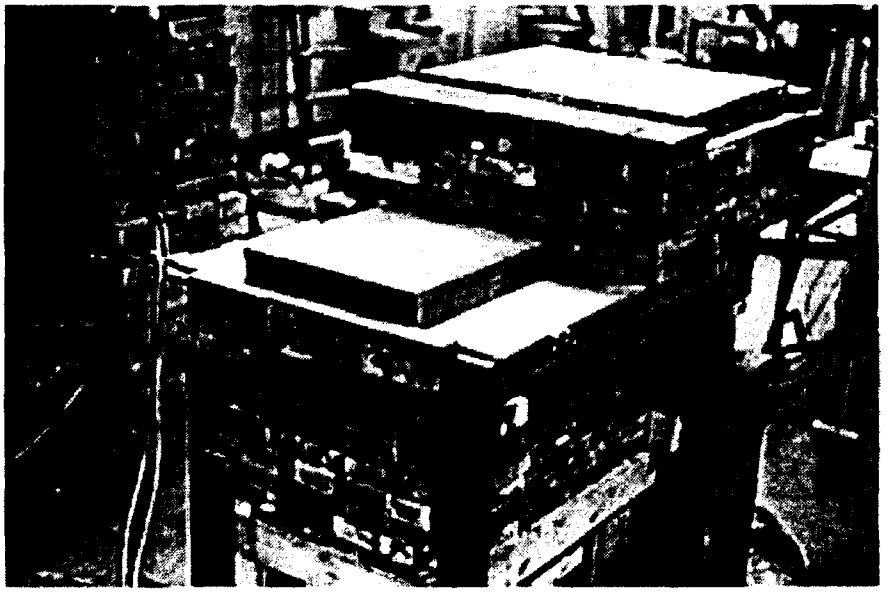

Figure 14. Photograph of the shielding around the detector collimators and signal detectors.

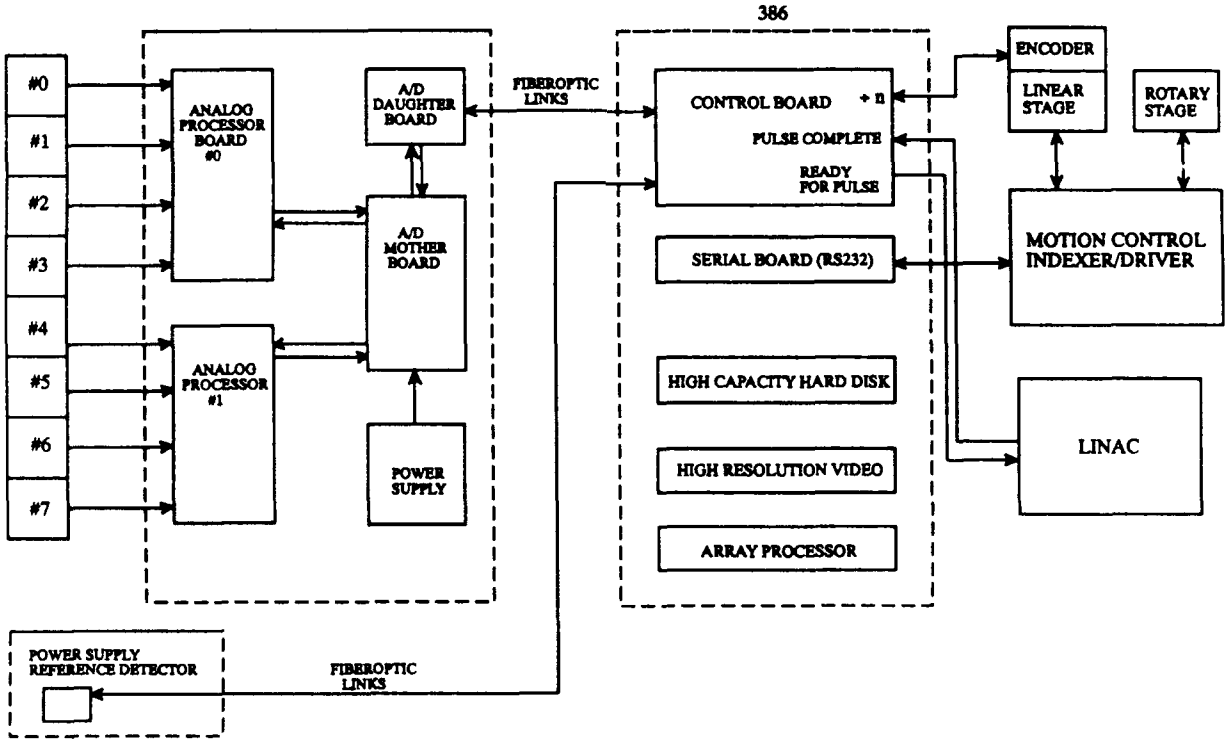

Figure 15. Schematic of data acquisition and control portion of supervoltage system.

3.3 Typical Scan and Image Parameters

Typical source settings were 60-MV peak energy (20-MV average energy) with a pulse rate of 100 Hz. The 4-mm by 25-mm fixed apertures achieved about 1.6 line pair per cm in-plane spatial resolution and a 12.5-mm slice thickness. The scan time of about 4 hrs resulted in an image noise of approximately 2% relative to the attenuation of the simulated propellant. Scans comprised 1024 samples per projection and 720 projections. Sample spacing and pixel size of 2 mm was used to obtain a 1024 x 1024 reconstruction of the 1.8-m phantom.

4.0 RESULTS

4.1 Artifact Reduction

After installation and alignment of the collimators and scanning mechanism, the source control electronics and DAAC hardware and software were commissioned by making numerous single traverse and multiple traverse partial scans of the phantom. Reliability tests were repeated at various fractions of full power to ensure that no detector or detector electronics damage was occurring.

One of the first complete scans of the phantom (Figure 16) provided convincing evidence that supervoltage CT is feasible but also appeared to verify the Phase I concerns that supervoltage attenuation measurements may be influenced by scatter, buildup and background in a way that limits useful CT measurements. Artifacts in Figure 15 include a shading from edge to center and bright crosses near the holes (no inserts were used in this scan). A density profile along a line passing through a diameter (Figure 17) should be relatively flat but instead shows a significant cupping artifact, especially near the steel walls. Also notable is the fact that the density inside the two 5.3-cm holes intersected by the profile should be zero but is instead about 25% that of the simulated propellant. Also disturbing was the fact that the density profile across the propellant/air boundary in the bore should be a sudden transition rather than the gradual slope evident in Figure 17. Even though the statistical noise in the image is only 2%, artifacts reduce contrast sensitivity to defects such as the cracks at the fin tips, which are not evident in Figure 17.

A number of improvements were made to the shielding around the source and detectors in an effort to reduce or eliminate the cause of the artifacts. The scan of the phantom without inserts was repeated, and the resulting image (Figure 18) is convincing evidence that the additional shielding was completely successful in eliminating artifacts . The small cracks at the fin tips are evident in Figure 18, as are slight density variations in the simulated propellant (these variations were expected because of nonuniformities in the cement-iron mixture). The cupping and cross-shaped artifacts seen in Figure 16 were eliminated, and the image has a generally sharper appearance. A density profile through a diameter (Figure 19) shows sharp density transitions from propellant to air and air values inside the 5.3-cm holes. That no cupping at all is seen is somewhat surprising but is explained by the facts that all measurements are made relative to the 30-cm iron beam stop filters and that, as shown in Figure 3, the mass attenuation coefficient of the simulated propellant is relatively independent of energies over the range of 10 to 30 MV (effective energies for a 60-MV peak bremsstrahlung source).

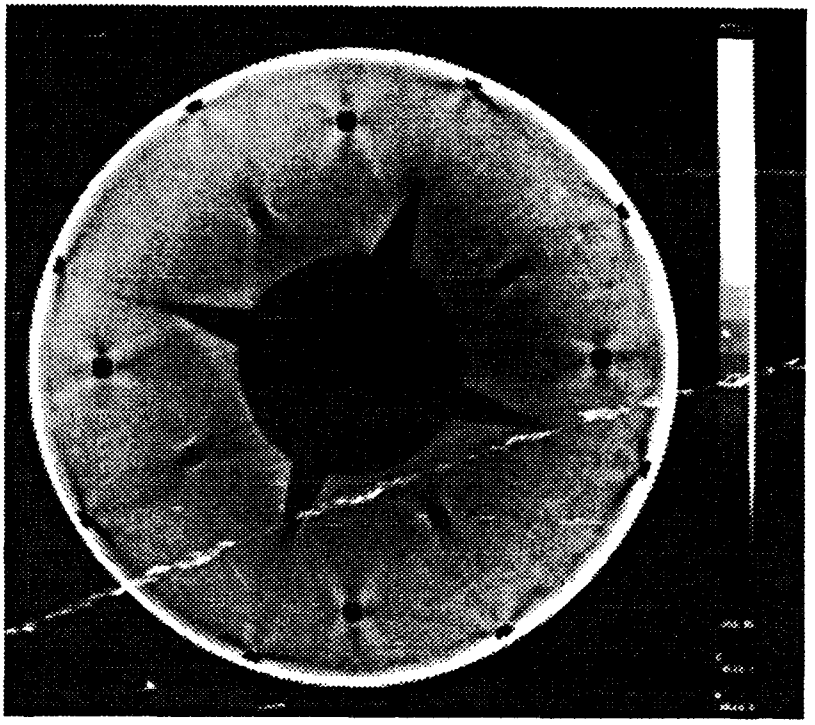

Figure 16. CT image of phantom without inserts before improving shielding.

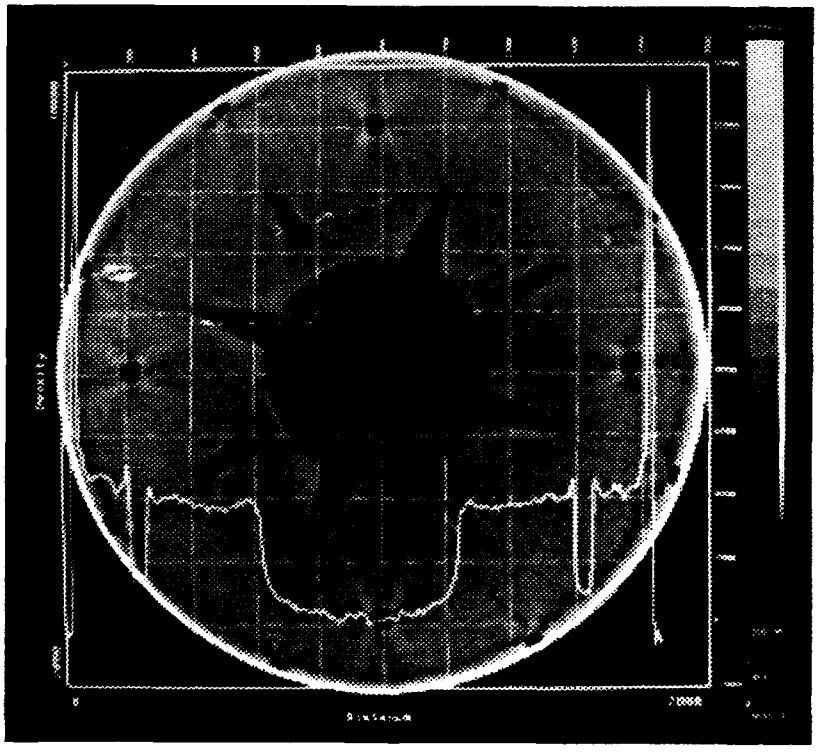

Figure 17. Density profile through CT image of phantom before improving shielding.

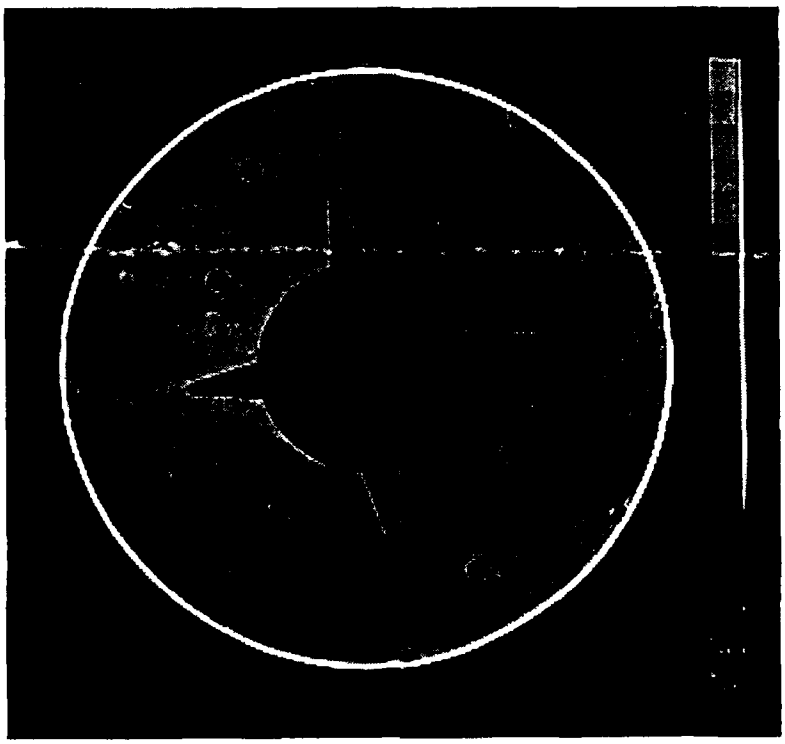

Figure 18. CT image of phantom without inserts after improving shielding.

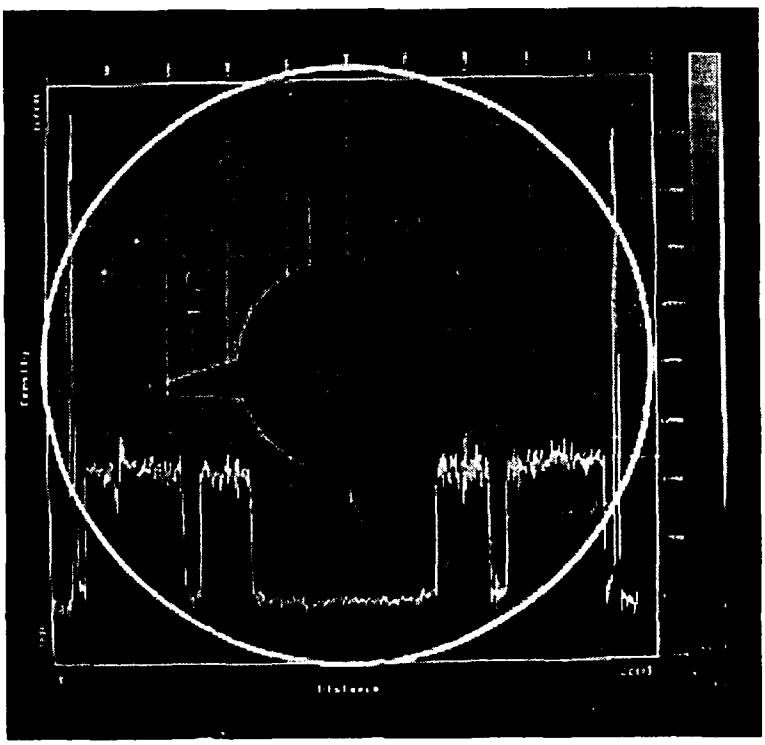

Figure 19. Density profile through CT image of phantom after improving shielding.

4.2 Density Resolution

As a test of supervoltage CT measurement flexibility, accuracy, and dynamic range, a number of inserts were placed in the holes in the phantom and the scan was repeated. The 5-cm inserts were wood, lucite, teflon, aluminum and titanium (Figure 20). Aluminum/Delrin debond simulations, constructed as shown in Figure 5, and ranging from 0.12 mm to 1.0 mm in width, were placed in the half-holes at the periphery. Aluminum was placed in several locations to check for spatial uniformity in the reconstructed image.

The inserts are clearly visible in the CT image (Figure 21), and the image is of the same high quality as that obtained without inserts. The aluminum inserts are all light grey, independent of their location the teflon dark grey and the titanium white. The 3-mm difference in diameter between the inserts and holes also is visible as a gap around, or to one side, of the insert. The spatial resolution was not sufficient to see debonds near the interface in this single slice but the possibility remains that the debonds may still be visible if multiple slices are viewed with advanced display capabilities.

The grey scale failed to show the difference between air, wood and lucite, all of which are black in this image. However, measurements of the reconstructed attenuations plotted as a function of theoretical attenuations (assuming an effective energy of 20 MV) do show that all materials were detected and that their measured values are correct over a dynamic range extending from wood to iron (Figure 22). The only material that deviates from linearity in Figure 22 is the iron/concrete mixture, but such a deviation was expected since the exact density of the mixture at the location of the measurement is not known (an average phantom density of 3.0 g/cc was used in the calculation of the theoretical attenuation coefficient).

The agreement between experiment and theory apparent in Figure 22 is conclusive proof that a properly designed and shielded supervoltage CT system can provide CT images of a quality equal to, if not better than lower energy CT systems.

As a further demonstration of the range and contrast sensitivity of supervoltage CT, a second set of materials were placed in the phantom (Figure 23). Included with these were a number of plastics of similar density but different elemental composition (nylon, lucite, PVC and ABS), two samples of inert propellant (one compressed using a metal band and one free standing), two water samples (one at 20°C and one at 80°C), three pieces of graphite (1.68, 1.83 and 1.86 g/cc), a magnesium block and a large watermelon. The graphite, magnesium and watermelon were arbitrarily arranged in the bore of the phantom.

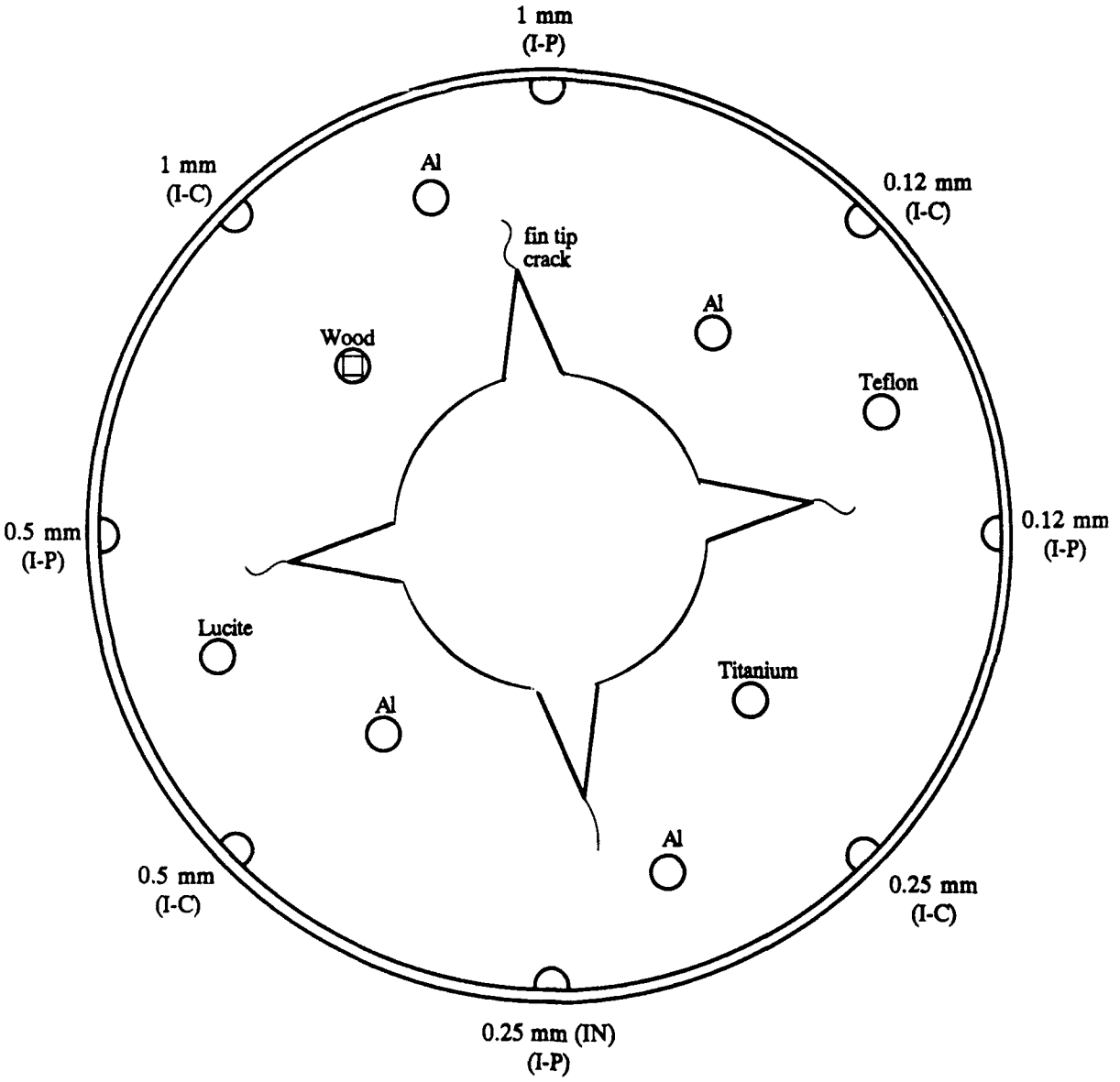

Figure 20. Schematic of phantom showing type and location of first arrangement of inserts

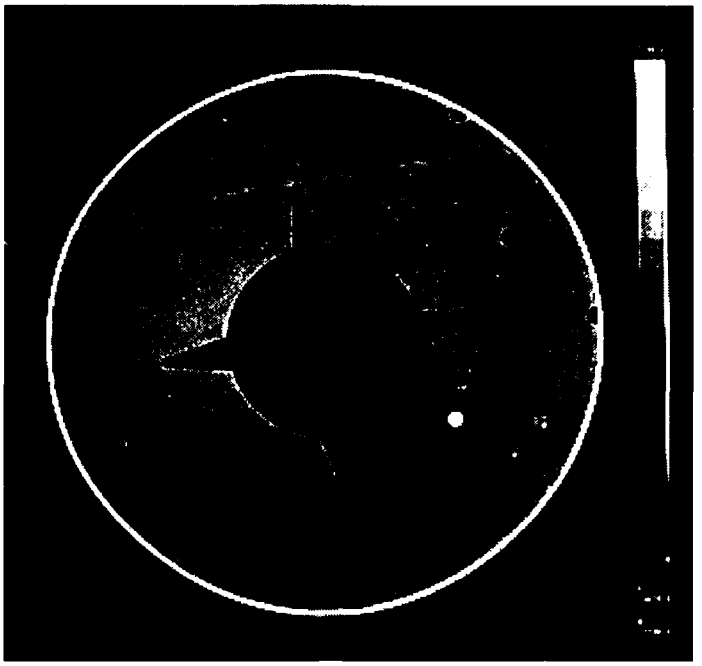

Figure 21. CT image of phantom with first arrangement of inserts.

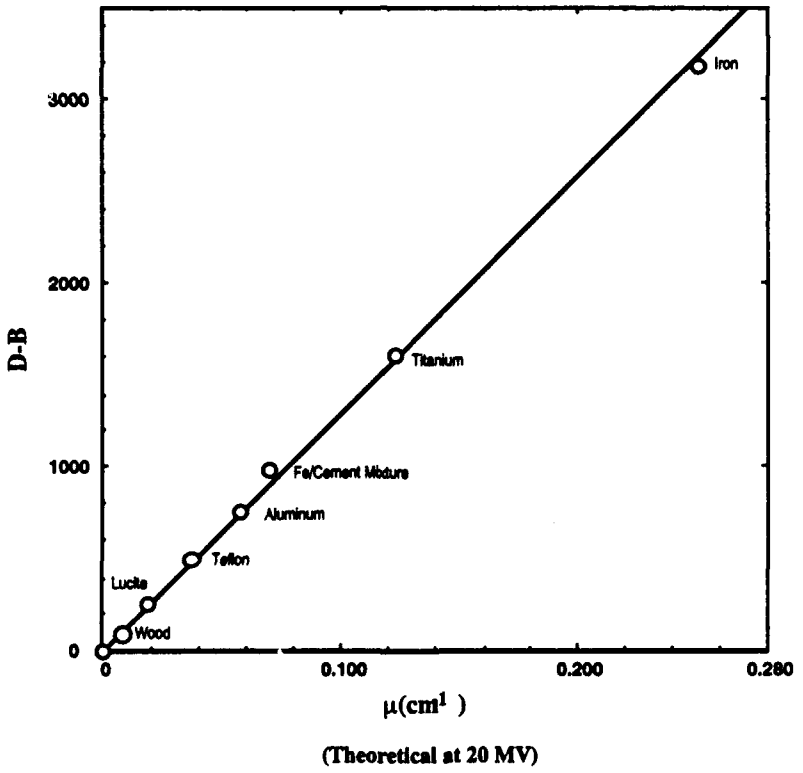

Figure 22. Measured linear attenuation coefficients as a function of calculated attenuation coefficients for the first arrangement of inserts.

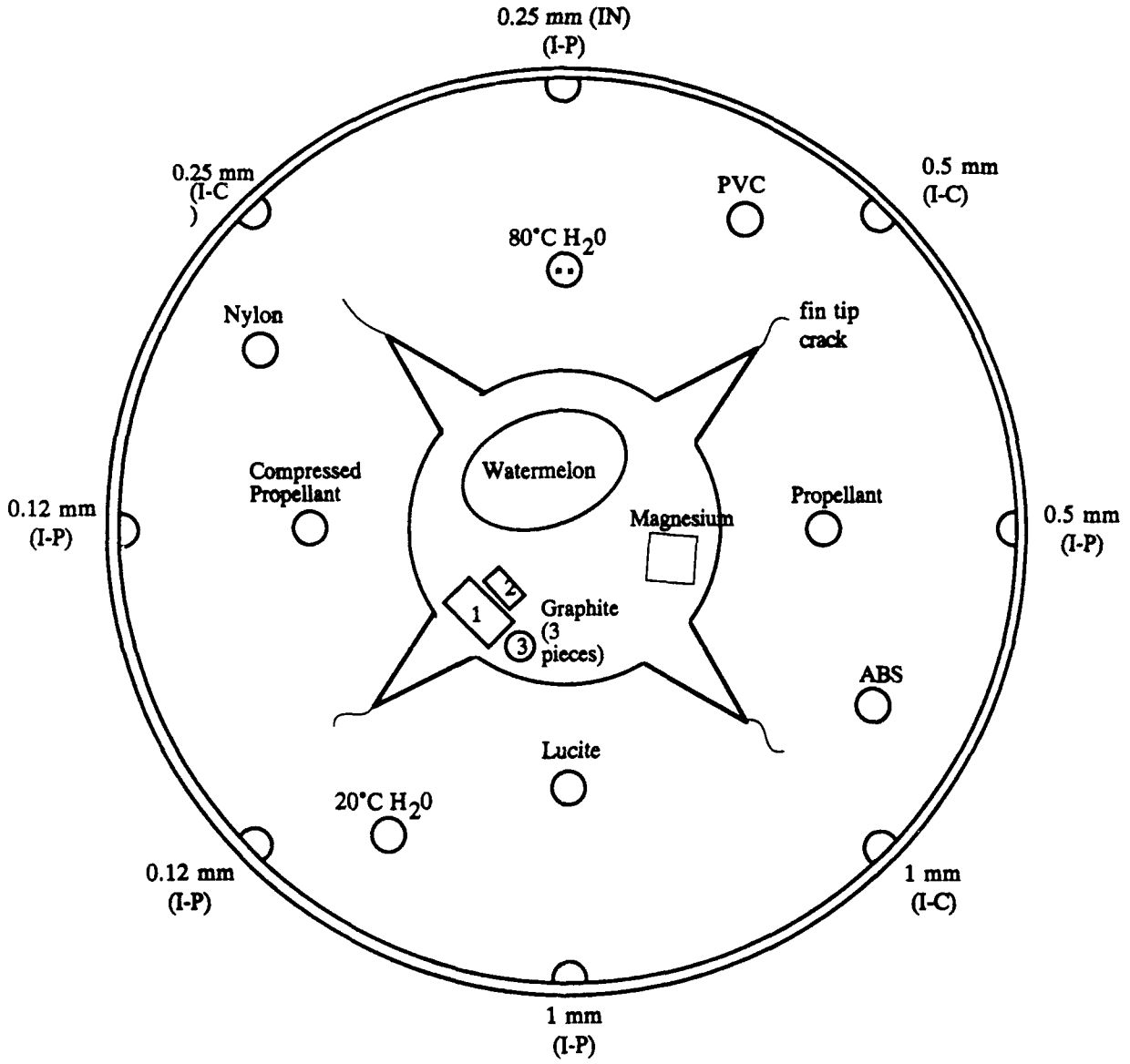

Figure 23. Schematic of phantom showing type and location of second arrangement of inserts.

The CT image (Figure 24) accurately represents all materials in the phantom, although many of the materials are so similar in density that pixel values had to be measured to detect the differences. The contrast in this image was stretched to highlight differences in densities in the 0.5- to 3- g/cc range at the expense of contrast between densities above 3 g/cc. Differences in density between the compressed and free standing propellant, the nylon and PVC, and the three graphite pieces are apparent. Note that, as expected, the magnesium density is very similar to that of the propellant. The heater wires used to keep one of the water samples at 80°C are seen in the image although pixel measurements were required to detect the small density difference between the 80°C water and 20°C (room temperature) water.

Measurements of the reconstructed attenuations plotted as a function of theoretical attenuations (assuming an effective energy of 20 MV) show that differences between even very similar materials were detected and accurately measured (Figure 25). Of particular note is the 2% decrease in the attenuation of 80°C water relative to 20°C water (the literature predicts a 2.6% reduction). This measurement graphically illustrates the counter-intuitive fact that small differences between materials can be accurately measured with supervoltage energies. In the case of the water samples, contrast is independent of energy since the two samples have exactly the same elemental composition (H_2O). The same is true of the three graphite samples, two of which differ in density by less than 2%, but all of which have the same elemental composition (C). In both cases, the contrast between attenuation values is due solely to differences in density; the mass attenuation coefficient is the same (because the elemental composition is the same and the energy is the same) and, therefore, does not contribute to contrast (see Figure 1).

The difference in attenuation between free standing inert propellant and compressed inert propellant also is due solely to a difference in density between the two samples. The propellant was compressed using a metal band which reduced its volume, and thus increased its density, by about 20%. The measured increase in attenuation is 19%. In another scan (not shown) a 50-kilogram weight was placed on the propellant otherwise free standing, resulting in an increase in attenuation of the propellant by about 8%. These scans suggest that density variations due to compressive loading in a large SRM's may be measurable using supervoltage CT.

A series of scans of sand samples were also performed. These samples ranged in density from 1.47 g/cc (loose sand) to 1.6, 1.67 and 1.73 g/cc (sand packed in closed vessel with increasing degrees of compaction). Scans were also done to investigate the density effects on sand near a piling driven in to the sand. Unfortunately, time did not allow a complete study but it was shown that the density of the sand does not increase around the sides of the piling. It is anticipated, however, that the sand density will be increased by the driving action directly under the piling. The significance of this work is that soil physicists and foundation engineers often study

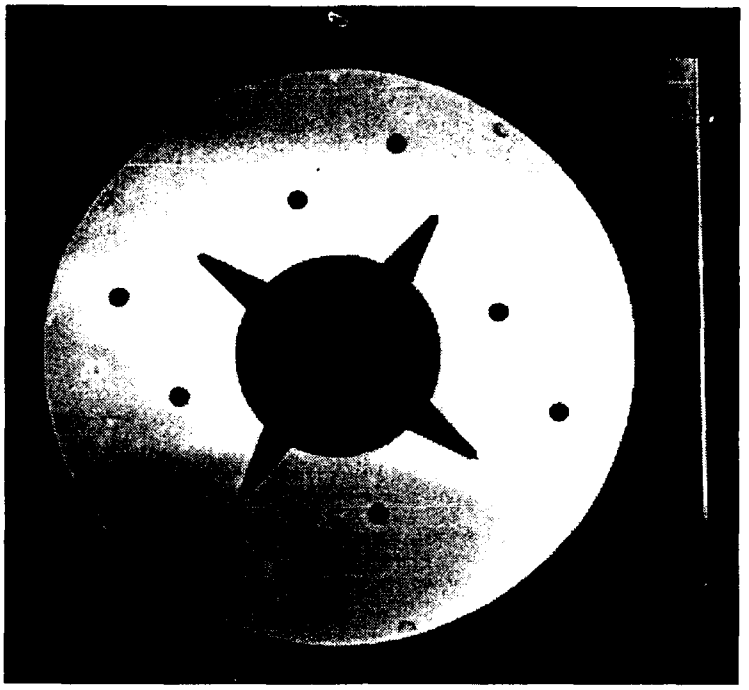

Figure 24. CT image of phantom with second arrangement of inserts.

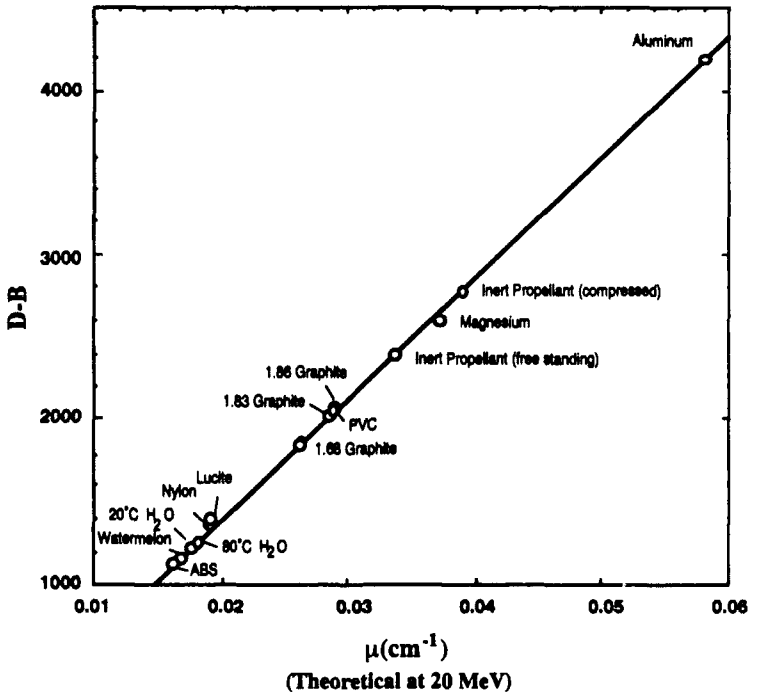

Figure 25. Measured linear attenuation coefficients as a function of calculated attenuation coefficients for the second arrangement of inserts.

the behavior of soil under load; and supervoltage CT offers, for the first time, the possibility of observing soil test structures totally nonintrusively. Supervoltage CT could handle test structures full of soil as large as 5 m in diameter.

A number of high density inserts in the phantom were also scanned. The inserts, which included titanium, iron, brass, tungsten and uranium, *combined with the phantom itself*, caused excessive absorption of the X rays and resulted in numerous artifacts in the image. Surprisingly though, useful relative attenuation measurements could still be made despite the artifacts. It is anticipated that supervoltage CT will be ideal for imaging many high density objects including jet engines, nuclear fuel bundles, nuclear waste containers and other objects containing high-Z materials when viewed separately in their own right.

A scan of the phantom with inserts was also taken at 40 MV to investigate the effect of supervoltage X-ray energy. The 40-MV image was similar in appearance to 60-MV scans, but linearity measurements revealed a slight increase in attenuation at the center of the image. A plausible reason for this effect is an increase in background due to the fact that lead shielding is less attenuating at 40 MV than at 60 MV.

In another scan the X-ray source current was increased from 15 μA to 45 μA in an effort to reduce the 2% noise (measured relative to the simulated propellant) without increasing scan time. As a result of the increased current, the noise was reduced to only about 1.5%, indicating the existence of nonphoton related noise. By comparing results and assuming that the nonphoton source of noise is Gaussian and does not vary with scan current, the nonphoton noise is estimated to be about 1%. The photon noise is estimated to be about 1.6% for the 15-μA scan and about 0.9% for the 45-μA scan. No detailed investigation of the source of the nonphoton noise was done, but it is anticipated that its causes can be eliminated with careful engineering. Possible causes include translation table jitter, focal spot motion, and source pulsing jitter.

4.3 Region of Interest Scanning

A region-of-interest (ROI) imaging method was also investigated as a means of detecting the simulated debonds at the periphery of the phantom without drastically increasing scan time. An important reason for SRM inspection is detection of debonds between the insulator and case (IC) and between the insulator and propellant (IP). If it is true that these debonds manifest themselves only as narrow, circumferential slits, very high spatial resolution will be required to detect them directly detectable in a CT image. Achieving high spatial resolutions, say pixel sizes of 1/4 mm, on an SRM 3 to 4 m in diameter requires data files as large as 16,000 rays per projection as well as approximately 12, 000 projections if conventional CT techniques are used. Even if the data could

be acquired at an acceptable rate, the many other problems associated with handling such large files make high resolution CT difficult by conventional means.

The ROI of interest in the SRM application is an annulus encompassing the IC and IP interfaces. Therefore, a possible ROI scan pattern for the interface regions of an SRM is a combination of high resolution scanning at the periphery and lower resolution scanning through the center (Figure 26). Note that, with many projections of this scan pattern, every point in the ROI is sampled at high resolution, but only in the tangential direction. All other sampling through any point in the ROI is at the lower resolution. This ROI sampling scheme is not adequate for arbitrarily shaped defects but is perfectly suited for tangentially oriented separations at the circumference. The reason for this is that narrow, tangential separations have virtually no effect on nontangential X-ray transmission measurements. Consequently, nontangential scanning can be low resolution without reducing CT sensitivity to circumferentially oriented slits. The ROI scanning technique illustrated in Figure 26 uses this fact to maximum advantage as a means of reducing the amount of data required to form a high resolution CT image that is sensitive to narrow, circumferentially oriented slits.

The ROI technique was tested for simulated IP and IC debonds of various thicknesses. The debonds were created using inserts (Figure 5) placed in the semicircular wells at the periphery of the phantom. Each insert comprised an aluminum semicircle (to simulate propellant) and a 4-mm thickness of Delrin plastic (to simulate insulator) sandwiched between the flat face of the aluminum and the inner surface of the case. Gaps machined on one side of the Delrin simulated IC or IP debonds, depending on which way the Delrin was inserted.

CT images of the simulated SRM show the steel case, shape and density variations of the simulated propellant, cracks at the fin tips, and inserts in circular wells at various locations in the SRM. However, even with digital magnification and density profiling (Figure 27), conventional, low resolution CT fails to reveal the 1-mm debond between the Delrin and aluminum.

A density profile through the high resolution ROI CT image obtained with 1.2-mm apertures (lead/foam sandwiches were inserted in the 4-mm apertures to reduce the effective aperture width) and 0.25-mm sample spacing reveals the 1-mm debond between the Delrin and aluminum (Figure 28). While the noise in the density profile is high, the low-density spike due to the 1-mm IP debond is statistically significant. A conventional CT image showing this detail would have required 4 to 8 times as much scanning and would have presented numerous data handling problems. Furthermore, this ROI technique obviates the need for high-resolution measurements in the highest attenuations (i.e., longest cords) near the center of the SRM. This is a big advantage if, as is true in this application, high resolution measurements could not be made through these highly attenuating cords because of low signal levels.

Volumetric 3-D display of many two-dimensional CT slices has been shown to greatly enhance the SRM debond sensitivity that can be realized using CT. A major difficulty with 3-D CT is the large quantity of data that must be collected and displayed. It is anticipated that ROI images can significantly reduce the total amount of data required for 3-D imaging and display of SRM's while at the same time maintaining or enhancing debond sensitivity.

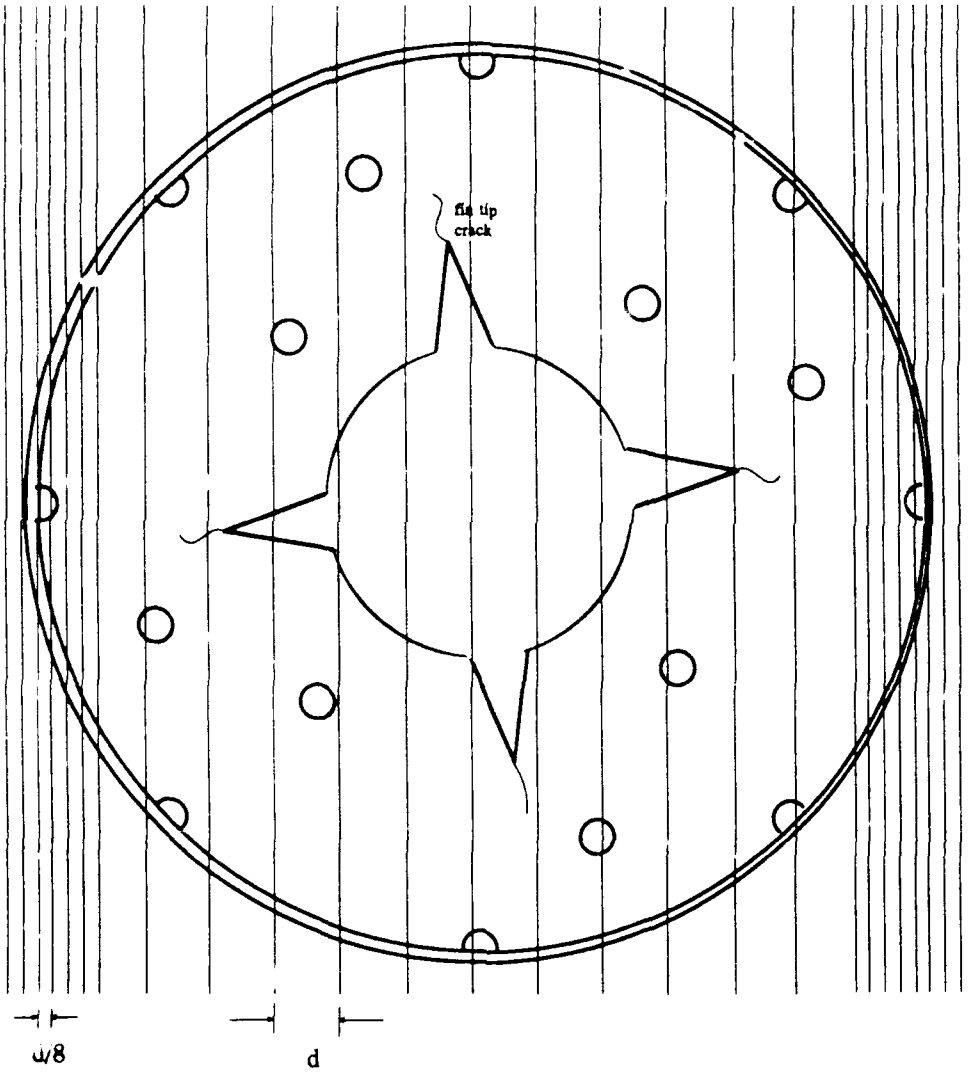

Figure 26. Schematic of high resolution region-of-interest scanning arrangement.

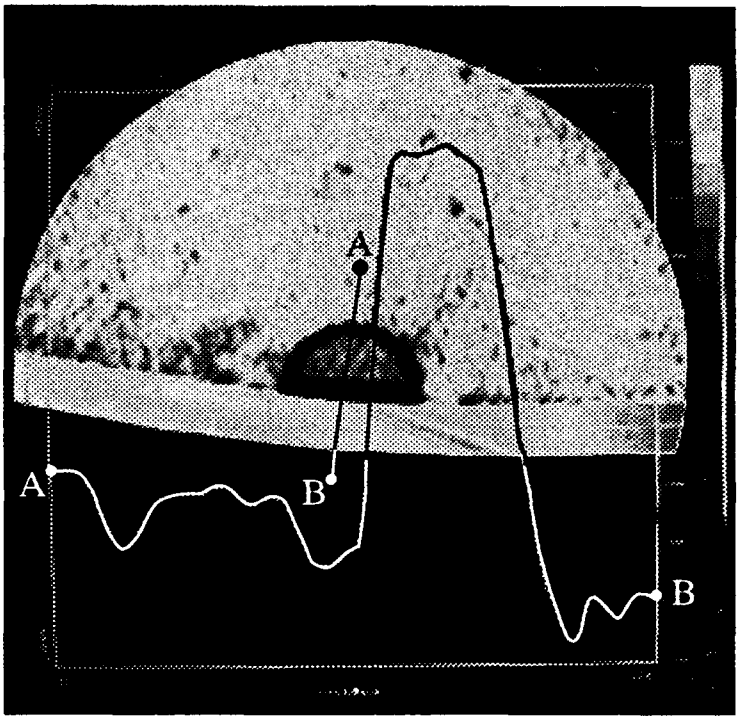

Figure 27. Density profile through 1 mm debond in 2-mm resolution CT image.

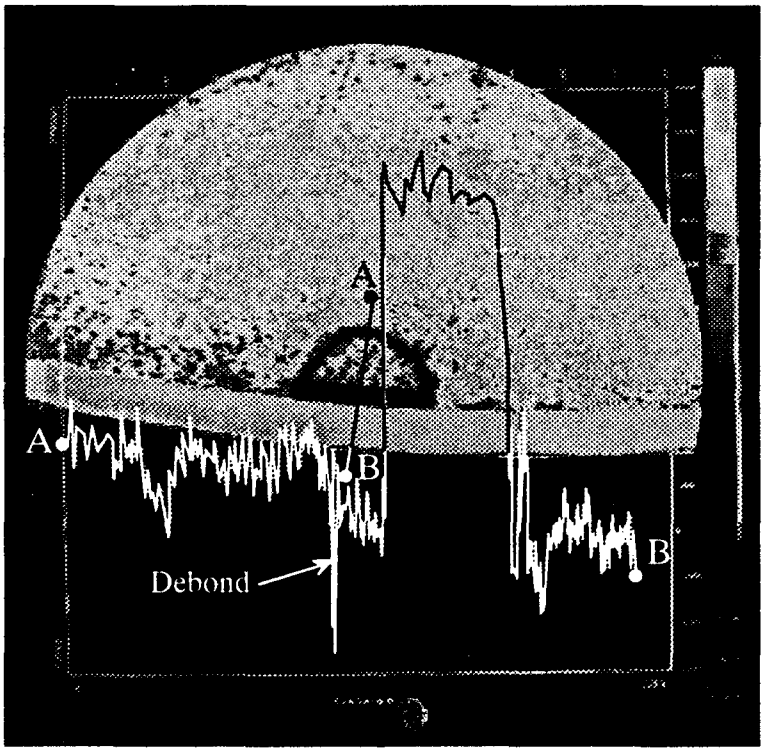

Figure 28. Density profile through 1 mm debond in high resolution ROI image.

5.0 CONCLUSIONS AND DISCUSSION

Recent catastrophic events in the aerospace community such as the Challenger and Titan rocket explosions serve to underline the need for the best available technology for inspection of advanced aerospace components. The field of nondestructive evaluation (NDE) has rapidly expanded in recent years with one of the newest and most significant developments being industrial CT. If the power of CT is to be extended to the largest aerospace components, even higher energies than the current maximum energy of 16 MV must be used. Supervoltage CT extends source energies to the point where no further increase in X-ray energy can provide improvements because, at energies above the supervoltage regime, the attenuation of materials increases prohibitively with energy.

The key objective of the Phase II supervoltage CT program was to obtain a supervoltage CT image of an aerospace structure that could not otherwise be imaged with current CT technology. This objective has been met and far surpassed by this project. It can be concluded that the extension of X-ray computed tomography to the highest possible energies is complete and verified. As a direct benefit, a new NDT technique, supervoltage CT, is available for the imaging of both high-Z and low-Z objects.

A total of 11 supervoltage images were obtained in the course of the experiment. The accuracy and sensitivity of the images is as good or better than most low-energy CT systems. Density profiles through the images indicated no cupping artifact, conclusive proof that, with proper shielding design, nonlinear effects such as beam hardening, build-up, scatter and background radiation can be virtually eliminated from supervoltage data. The high quality of these images is also conclusive proof that, with proper design, problems posed by the large dynamic range of the X-ray signal can be dealt with. Very subtle features such as fin tip cracks, density irregularities in the cement/iron mix and small gaps between inserts and holes are all visible and reliably imaged, independent of the orientation or selection of inserts used with the phantom. This achievement is all the more remarkable in view of the fact that the same claim cannot be made about many low energy CT scanners currently being marketed

The flexibility of supervoltage CT was demonsrated using many different combinations of inserts. The inserts were faithfully represented in the supervoltage images and detailed attenuation measurements confirmed that the attenuation coefficients were accurately measured. Density differences of 1 to 2% between samples of graphite, samples of sand and even between water at 20°C and 80°C were correctly measured, proving conclusively that contrast resolution is not diminished at supervoltage energies.

Samples of inert propellant were scanned and, as an example of the utility of supervoltage CT, the change in density of the propellant due to various degrees of compressional loading was measured. The excellent results achieved indicate that in addition to defect detection in steel wall SRM's up to 4 m in diameter, supervoltage CT might be able measure small density changes caused by variations in compressional force loading in the SRM.

Enhanced contrast sensitivity can also be realized at supervoltage energies because of the increased contrast between mass attenuation coefficients in the supervoltage regime. For example, the magnitude of the demonstrated contrast between a sample of PVC and a sample of nylon is significantly greater at an effective energy of 20 MV than it is a 5, 2 or 0.5 MV. In fact the same contrast could only be achieved at energies below 0.070 MV. However, at 0.070 MV, no X-rays would be able to penetrate objects even a fraction of the size of the supervoltage phantom.

The enhanced contrast effect strongly suggests that it should be possible to obtain two separate, low-noise images: one primarily sensitive to elemental composition and the other primarily sensitive to density distribution, using a supervoltage dual-energy technique. This technique would be similar to the dual-energy technique performed at lower energies, except for the fact that it would not be hampered by a lack of adequate photon statistics nor be restricted to smaller, low-Z objects. Possible applications for an SVCT dual-energy technique include, but are not limited to, the detection of chlorine migration and aging effects in SRM propellant, the detection and in-process monitoring of elemental composition distributions in advanced ceramics and composites, the detection of residual core in cast turbine blades, the migration of fluids and high-Z components in soil test beds, the inspection of nuclear fuel waste drums, the detection of explosives, munitions and contraband in rail cars luggage and the detection of corrosion-related aging effects in aircraft.

A region-of-interest (ROI) imaging method was also demonstrated as a means of detecting the simulated debonds at the periphery of the phantom without drastically increasing scan time. An important reason for SRM inspection is detection of debonds between the insulator and case and between the insulator and propellant. If it is true that these debonds manifest themselves only as narrow, circumferential slits, very high spatial resolution may be required for them to be detectable in a CT image. Achieving high spatial resolutions, say pixel sizes of 1/4 mm, on an SRM 3 to 4 m in diameter would require data files far in excess of current computer capabilities if conventional CT techniques were used. Even if the data could be acquired at an acceptable rate, the many other problems associated with handling files that large would make conventional high resolution CT difficult, if not impossible at this time.

Using the ROI technique, a 1-mm debond between the simulated insulator and propellant was detected, where detection of the same debond without the ROI technique was clearly not possible. A conventional CT image capable detecting the 1-mm debond would have required 4 to 8 times as much scanning and would have presented numerous data handling problems. Furthermore, the ROI technique obviates the need for high-resolution measurements in the highest attenuation cords (i.e., longest cords) near the center of the SRM. This is a big advantage if, as is true in the SRM application, high resolution measurements could not be made through the longest cords because of low signal levels.

The main engineering issues concerning proceeding to full-up design of a supervoltage CT system are the reduction of the 1% nonphoton related noise level by a factor of 10 and the identification of a commercially available source. Since it is likely that at least some of the non-photon noise originates with the source and source pulsing arrangement, the use of a commercially available supervoltage linac may result in a major noise reduction on its own. Other possible sources of nonphoton noise such as translation jitter and detector electronics, can be engineered for optimum noise reduction (little or no noise level optimization was done for the Phase II experiment).

The recent emergence of commercially available linear accelerator sources in the supervoltage energy range is an important development that will greatly enhance the practicality and effectiveness of supervoltage CT. As a first step in Phase II follow up, the performance of supervoltage sources should be characterized in cooperation with the source manufacturers to determine their suitability for supervoltage CT.

APPENDIX

EXPERIMENTAL SCHEDULE AND TEST PLAN
(abridged version of the Technical Operating Report submitted March 25, 1990)

The proposed schedule for the experimental portion of the SVCT contract (Figure A1) calls for receipt of the SVCT equipment at the RPI Linac by June 4, 1990 and completion of all experiments and return shipment of equipment by June 30, 1990 . At time of writing, two major deliverables, the rotating table and the translating table have not yet been received at ARACOR and, as a result, data acquisition and control software has not yet been finalized. It has been confirmed that these items will be delivered to ARACOR on schedule (on or before April 15) and no slippage is anticipated.

Other than the June 4 start and June 29 completion, dates provided in the schedule are intended for planning purposes only and may be modified as required during the experiment. The June 4 and 29 dates may also be changed slightly to accommodate personnel schedules, RPI facility schedules, etc., but, at least initially, are presented as firm dates around which plans will be generated.

The items in the following test plan (Table A1) are listed in the same order as shown in Figure A1. The general test plan strategy is to move as quickly as possible toward the prime objective of obtaining a CT image of the phantom. Scans of the phantom in other configurations, and characterizations of the effect of aperture l/d, source energy and scan pattern will be pursued to the extent that time and money allow.

The phantom will be equipped with inserts to facilitate the determination of spatial resolution, contrast resolution and CT linearity. Inserts will also contain simulated debonds, voids, cracks and inclusions. In general, these inserts will be removable and interchangeable, to facilitate testing for positional dependent effects that may or may not exist.

Table A1. SVCT Test Plan.

1. RECEIVE COMPONENTS

- ship components for receipt at RPI on Monday, June 4
- ARACOR personnel to be notified on receipt and fly out for Monday set-up tasks

2. SET UP

- attempt to measure size and location of focal spot
- align collimators and positioning equipment
- set up data acquisition equipment
- connect source trigger and test

3. TEST HANDLING SYSTEM MOTION

- test mechanical motion without phantom

4. TEST REFERENCE DETECTOR

- measure signal with source off
- measure signal with source on, detector set at lowest elevation
- raise detector to achieve acceptable signal level
- check operation at 40 and 60 MV

5. TEST SIGNAL

- measure signal with source off
- check stability
- measure air value with source on
- set gains
- check detector collimator alignment to test effect on signal level
- check temporal stability
- check statistical behavior
- measure for various lengths of time, check for Gaussian behavior
- attempt to measure and calculate photons/cm^2/s for both energies

Table A1. SVCT Test Plan (Cont'd).

6. IMPROVE DETECTOR SHIELDING

- measure signal with source on, apertures blocked
- adjust shielding if necessary
- check for change in signal with significant object mass on table
- adjust shielding if necessary

7. CALIBRATE DETECTORS

- measure air values for both aperture widths
- adjust gains as required
- measure temporal behavior and stability
- measure signal linearity using known attenuator lengths

8. CALIBRATE FOR GEOMETRY

- locate handling system motion axis perpendicular to the X-ray beam
- locate handling system center relative to collimators

9. LOAD PHANTOM

- check mechanical motion
- check source on-aperture closed signal variability
- check aperture-open measurements
- check reference detector signal stability

10. CT SCANS (by phantom)

- Select aperture size, collimator length & points per projection.
- Collect 180 degrees of data with 90 traverses (0.25 degree projection spacing).
- Preprocess data at the end of each traverse and display sinogram at end of each traverse.
- Reconstruct image data at the end of the sequence of traverses.
- Display and evaluate image.
- Adjust collimator lengths and repeat CT scan of phantom if warranted by image quality.
- repeat for other configurations of test phantom

Table A1. SVCT Test Plan (Cont'd).

11. CT SCANS (by aperture length)

- perform CT scans with reduced aperture lengths of both source and detector
- perform CT scans with source aperture length reduced in stages
- leave detector-side sections of source collimator in position while removing others

12. CT SCANS (by aperture width)

- collect a complete higher resolution CT image
- collect portions of higher resolution images
- check for reduction in in-plane scatter as aperture width is reduced

13. CT SCANS (by source energy)

- test the effect of different source energy on noise level
- test the effect of different source energy on in-plane scatter level

14. OTHER TESTS

- perform other CT scans or tests conceived of in the course of the experiment

15. DISMANTLE

- dismantle and pack equipment for shipment
- arrange for the temporary storage of any equipment that may be radioactive

16. SHIP

- ship components by Friday, June 29
- ARACOR staff return flight

TASK	June 1990					
	1 (Fri)	4 to 8	11 to 15	18 to 22	25 to 28	29 (Fri)
1. Receive Components at RPI	x					
2. Set Up		x				
3. Test Handling System Motion		x				
4. Test Reference Detector		x				
5. Test Signal		x				
6. Improve Detector Shielding		x				
7. Calibrate Detectors		x				
8. Calibrate for Geometry		x				
9. Load Phantom		x				
10. CT scans (by phantom)						
10.1 configuration 1			x			
10.2 configuration 2			x			
10.3 configuration 3			x			
10.4 configuration 4			x			
10.5 configuration 5			x			
11. CT scans (by phantom)						
11.1 configuration 1				x		
11.2 configuration 2				x		
11.3 configuration 3				x		
11.4 configuration 4				x		
11.5 configuration 5				x		
11.6 configuration 6				x		
12. CT scans (by aperture width)					x	
13. CT scans (by source energy)					x	
14. Other Test (to be determined)					x	
15. Dismatle					x	
16. Ship Components to ARACOR						x

Figure A1. The proposed schedule for the experimental portion of the SVCT contract.